A CASE STUDY OF WEATHER RESEARCH AND FORECASTING MODEL OVER THE MIDWEST USA

BY

KAN FU

THESIS

Submitted in partial fulfillment of the requirements
for the degree of Master of Science in Environmental Engineering in Civil Engineering
in the Graduate College of the
University of Illinois at Urbana-Champaign, 2016

Urbana, Illinois

Advisers:

Dr. Sotiria Koloutsou-Vakakis
Professor Mark J. Rood

Abstract

Chemical Transport Models (CTMs) are important tools for air quality research, and it is of the same importance to provide accurate weather information as input data to CTMs. In this thesis, the Weather Research and Forecast (WRF) model was used as an input to a CTM and a sensitivity analysis of 17 WRF runs was conducted to explore the optimum physics configuration in 6 physics categories for the Midwest USA in May 2011, including cumulus, surface layer, microphysics, land surface model, planetary boundary layer, longwave radiation and shortwave radiation. Two domains were used: the coarse domain (12 km grid size) covering most parts of the North America and the nested domain (4 km grid size) covering the Illinois State and adjacent areas. The model output from the nested domain was evaluated statistically and results were compared with observation data using the Model Evaluation Tools (MET) software package and the National Center for Atmospheric Research Command Language (NCL). Benchmark values of several weather variables from the literature were adopted as a reference when discussing model statistical performance. After the sensitivity analysis was finished, the same optimum physics configuration for May was evaluated for October using measured meteorological data to test the applicability of the WRF model during different weather conditions. Finally, both the coarse domain and the fine domain were evaluated to investigate model sensitivity to the horizontal resolution.

Compared with the starting run, the optimum run was found to produce better temperature (0.35 K decrease in hourly mean bias and 0.26 K decrease in hourly root mean square error), pressure (4.3 Pa decrease in hourly mean bias and 3.91 K decrease in hourly root mean square error) and relative humidity (1.44 % decrease in hourly mean bias and 1.76 % decrease in hourly root mean square error) results, while keeping the ability to simulate wind speed and wind direction accurately compared with other studies. In addition, all the statistical measures were within the benchmark value ranges that were available in the literature (Emery et

al., 2001). When applying the same optimum physics configuration to October, WRF still produced acceptable results, with only gross error of wind direction out of the benchmark value range in hourly statistics (30.02° compared with 30° from the benchmark value). Comparison between the coarse domain and the fine domain suggested that decreasing horizontal resolution did not necessarily lead to increasing the model simulation skill.

The unique contribution of this research is to provide a general method of sensitivity analysis in WRF and obtain the optimum WRF physics configurations for the Midwest USA. These contributions are important because CTMs need accurate weather inputs to produce reliable outputs, and it is not easy to find the optimum WRF outputs given that there are many choices to make when running WRF.

To my father and mother, who gave me life and supported me unconditionally.

Acknowledgements

I would like to thank Dr. Sotiria Koloutsou-Vakakis and Professor Mark J. Rood for giving me the opportunity to work in the nitrogen project and for the support and guidance when I was struggling with the research and writing. Everything I learnt from them will be my life-long experience.

I also feel honored to be in the Nitrogen group and Air Quality Engineer and Science (AQES) group. Group members are cordial and friendly, and I enjoy attending group meetings to know them better and make them know me better, both in an academic way and non-academic way. Special thanks to my senior colleague, Srinidhi Balasubramanian, who I worked closely with and patiently gave me advice when I felt lost in the research.

Table of Contents

CHAPTER 1: INTRODUCTION

1.1 Research Context and Background

This thesis is a component of research to quantify the effects of ammonia (NH_3) emissions from agricultural fertilization to regional air quality. First, the broader background and context of the research are presented, followed by detailed description and presentation of model performance and sensitivity analysis for the Weather Research and Forecasting (WRF, Skamarock et al., 2008) model for the US Midwest region. WRF provides the meteorological parameters needed for running Chemical Transport Models (CTMs), which can be used to predict regional air quality.

1.1.1 Nitrogen in the Environment

Nitrogen, in the form of amino acids, nucleic acids and proteins, is one of the most essential chemical elements in the world to sustain life on Earth. It has an abundant source as N_2 in the ambient air, at 79% by volume, but is not readily available to most of living organisms due

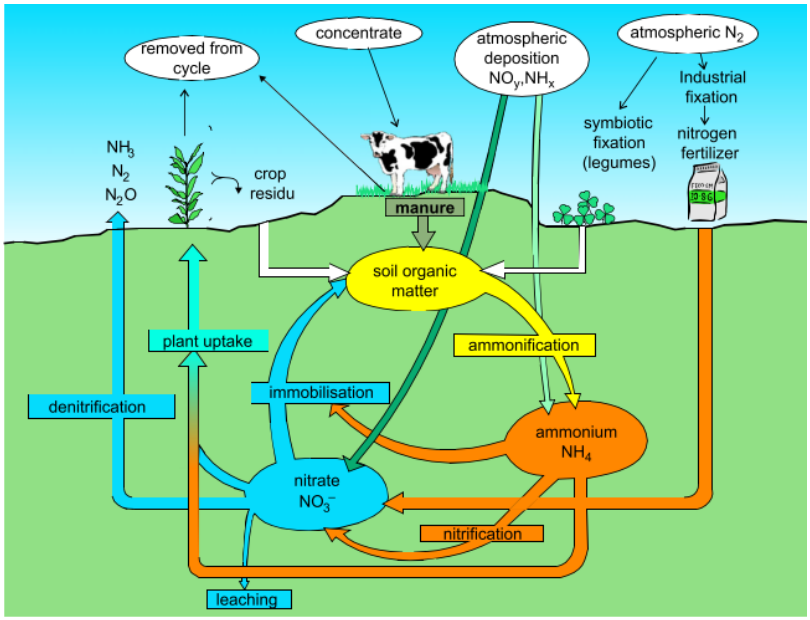

Figure 1.1 Schematic of the nitrogen cycle (Erisman et al., 2007).

to the strong nitrogen-nitrogen triple bond in its molecular dinitrogen form. The gaseous nitrogen (N_2) is inert under typical atmospheric conditions but can turn into reactive forms under conditions of high energy (e.g., high temperature and/or high pressure conditions such as lightning) or by some specialized nitrogen fixing bacteria (Galloway et al., 2003; Erisman et al., 2007). Reactive nitrogen (Nr) is defined as all the nitrogen compounds except N_2, including inorganic reduced nitrogen (NH_3 and NH_4^+), inorganic oxidized nitrogen (NO_x, HNO_3, N_2O and NO_3), and organic compounds (such as urea, amines, proteins, nucleic acids). NO_x describes the sum of nitrogen oxide (NO) and nitrogen dioxide (NO_2), and NH_x describes the sum of ammonia (NH_3), and ammonium (NH_4^+).

The nitrogen cycle describes how the nitrogen element is converted and transferred into different chemical forms through its reservoirs in the atmosphere, hydrosphere, geosphere and biosphere (Spiro et al., 2003). A schematic for the nitrogen cycle is shown in Figure 1.1 (Erisman et al., 2007). In nature, the most common ways to convert nonreactive N_2 into Nr are from lightning and biological nitrogen fixation. In the first case, NO_x is formed through lightning, which can become nitric acid (HNO_3) and be transported into the soil by atmospheric wet or dry deposition; in the second case, nitrogen fixing bacteria living in the nodules of legumes convert N_2 to NH_3. NH_3 can further be converted to nitrate (NO_3^-) through nitrifying bacteria. In this process, NH_3 is first converted to nitrite (NO_2^-) by nitrosomonas, then to NO_3^- by nitrobacters (Gao et al., 2015). Both NH_3 and NO_3^- can be absorbed by plant uptake for biosynthesis to make amino acids, DNA and RNA (Erisman et al., 2007). Human and animal waste and dead animals and plants produce NH_3 when they decompose. Finally, denitrifying bacteria close this cycle by reducing nitrates back to N_2 gas, with possible by-products of NO_2^-, NO and nitrous oxide (N_2O). In short, the nitrogen cycle is a series of complex biogeochemical processes (Erisman et al., 2007).

One notable fact about the nitrogen cycle is that this cycle had been very stable without humans' interference until the early 1900s. The reason is that Nr is not accumulated in nature due to the similar rates of fixation and denitrification (Galloway et al., 2003). However, with the invention of the Haber-Bosch process that enabled the conversion of N_2 to NH_3 for the production of fertilizers (Sutton et al., 2008; Ribaudo et al., 2011), the nitrogen cycle had been changed a lot. Figure 1.2 (U.S. EPA, 2011) shows the total emission of Nr to the atmosphere from different sources in the United States, in 2002. Most of the Nr generated in the United States is due to human activities, with the biggest part belonging to the Haber-Bosch process. Galloway et al. (2003) estimated that Nr production rate by human activities has increased from 15 Tg per year in 1860 to about 165 Tg per year in 2000. The change is essential to sustain food production for the growing human population. However, accumulating Nr in the environment can lead to severe environmental problems, including eutrophication, acidification of lakes and soils, fine particulate matter ($PM_{2.5}$, particles with diameter less than or equal to 2.5 μm) formation, stratospheric ozone depletion and global climate change (Vitousek et al., 1997; Galloway et al., 2003).

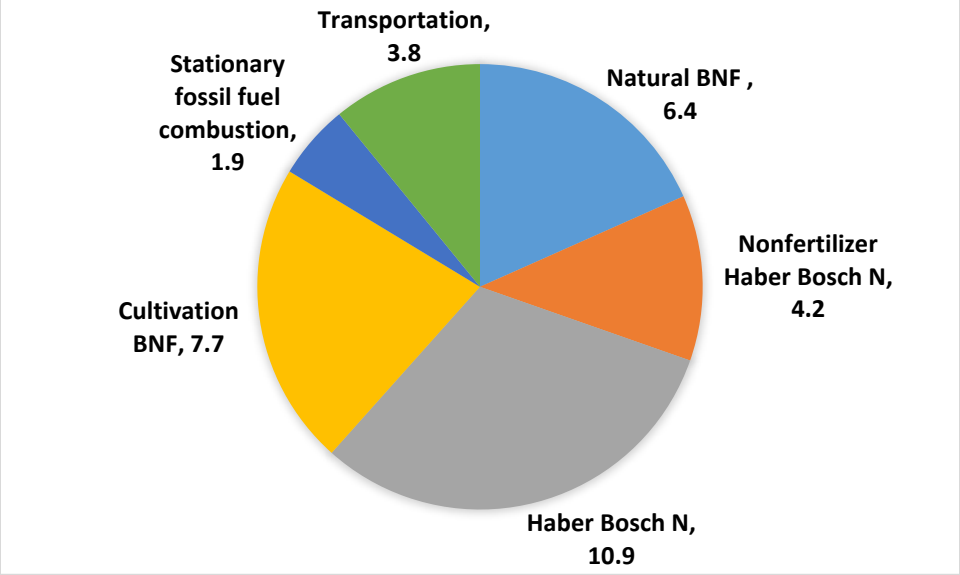

Figure 1.2 Sources of Nr emissions in the United States in 2002 (U.S. EPA, 2011). BNF: Biological Nitrogen Fixation; Unit: Tg N/yr.

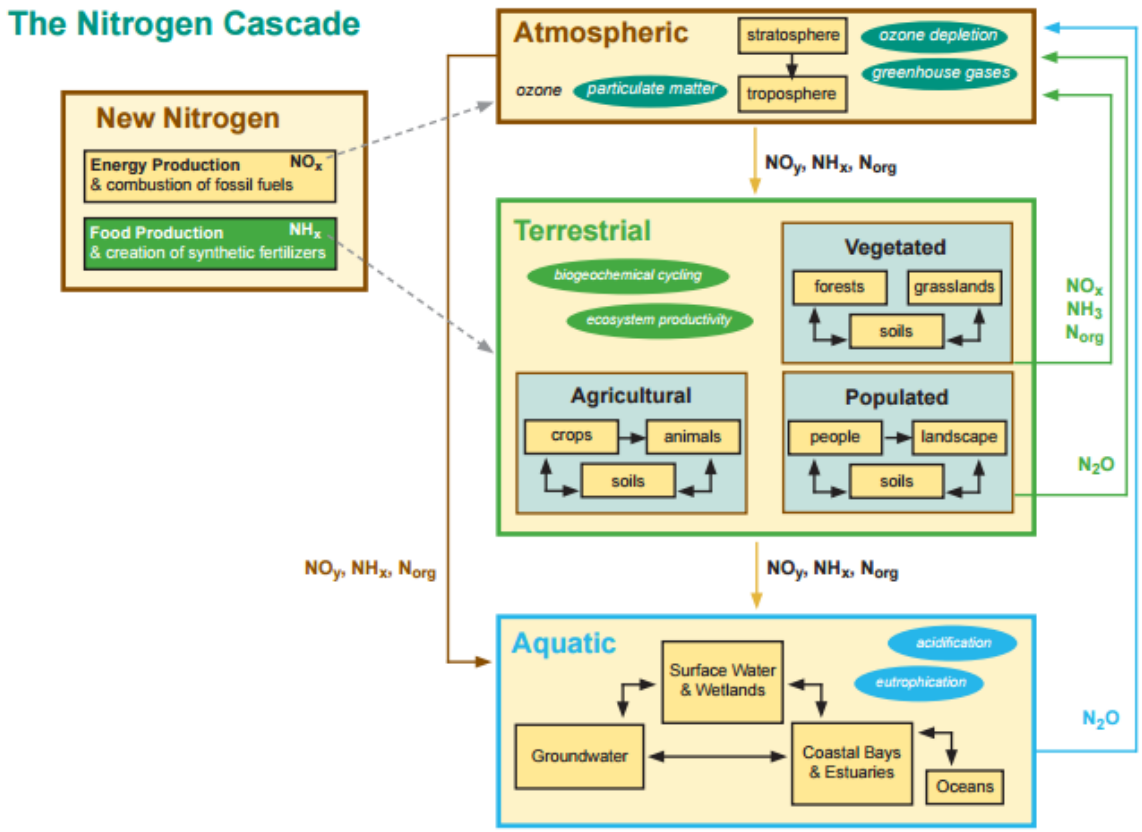

Figure 1.3 Schematic of the nitrogen cascade (U.S. EPA, 2011).

The term nitrogen cascade was introduced by Galloway et al. (2003) to describe the sequence of ecological and human health effects, as Nr molecules change and move from one ecosystem to another (e.g., terrestrial systems, aquatic systems and/or the atmosphere). Figure 1.3 (U.S. EPA, 2011) demonstrates the concept of nitrogen cascade, especially in the flow of new Nr generated from human activities. With regard to impacts of the nitrogen cascade in the atmosphere, new inputs of Nr from human activities to the atmosphere include NO_x mainly from fossil fuel and biomass combustion, and NH_3 and N_2O mainly from agricultural activities. In the atmosphere, NO_x can react with Volatile Organic Compounds (VOC) to form ozone and photochemical smog, both of which can decrease visibility, damage plant growth and cause severe respiratory problems to humans (Brunekreef et al., 2005). NO_x can also be converted into HNO_3. NH_3 forms Particulate Matter (PM) after reaction with sulfuric, nitric, or other inorganic and organic acids. Eventually, primary and secondary Nr products are removed from the

atmosphere through wet or dry deposition and enter terrestrial and aquatic ecosystems where in some cases can be beneficial, such as in areas with nitrogen poor soils. However, in other ecosystems, the excess Nr from the atmosphere can contribute to worsening of problems such as acidification and eutrophication (Erisman et al., 2013). N_2O, on the other hand is slightly reactive in the troposphere and with a lifetime in the atmosphere of 114 years. N_2O is a potent greenhouse gas with global warming potential 300 times higher than that of carbon dioxide (U.S. EPA, Climate Change, 2016). N_2O can also contribute to stratospheric ozone depletion. According to Ravishankara (2009), of all the stratospheric ozone depletion contributors from anthropogenic emissions, N_2O is and will be the most significant factor in the 21st century in place of the once dominant contributors, chlorofluorocarbons.

1.1.2 Atmospheric Chemistry of NH_3 and Related Environmental Problems

In the early 1900s, Fritz Haber and Carl Bosch developed the Haber-Bosch process to produce NH_3 from H_2 and N_2 gas under high temperature and pressure in large quantities (eq. 1.1, Sutton et al., 2008; Ribaudo et al., 2011).

$$N_2 + 3H_2 \xrightarrow{metal\ catalyst,\ \ high\ temperature,\ \ high\ pressure} NH_3 \qquad \text{(Eq. 1.1)}$$

Since then, anthropogenic NH_3 emissions (measured as teragram nitrogen) have increased dramatically, from 0 Tg N per year, before 1910, to over 100 Tg N per year, in 2000 (Galloway, 2003). Use of fertilizers results in NH_3 volatized from the field. Smil (2002) found that of all the fertilizers applied to the field, about half nitrogen is incorporated into the plant biomass, and the ratio can even go down to 40% to 60% in flooded rice fields where urea are directly applied.

1.1.2.1 Particulate Matter Formation

There are several chemicals that can react with NH_3 to produce particles, mainly in the form of ammonium sulfate and ammonium nitrate (U.S. EPA, 2011). In anhydrous environment,

NH_3 and SO_2 react to produce NH_3SO_2 or $(NH_3)_2SO_2$, depending on the stoichiometric ratio of the two reactants (eq. 1-2, eq. 1-3).

$$NH_3 + SO_2 \leftrightarrow NH_3SO_2 \quad \text{(Eq. 1.2)}$$

$$2NH_3 + SO_2 \leftrightarrow (NH_3)_2SO_2 \quad \text{(Eq. 1.3)}$$

The two reactions are reversible and the solid products can react back to their precursors when the gas pressure is low (Behera et al., 2013).

SO_2 can also be oxidized in both gas phase and liquid phase. In gas phase, SO_3 is produced when OH and peroxy radicals are present. Although the reaction rate of SO_3 with NH_3 is faster than that with water vapor, with 4 orders of magnitude difference (Behera et al. 2013), water is still the main reactant with SO_3 considering concentration difference in the atmosphere (6 orders of magnitude). In liquid phase, SO_2 is converted to SO_4^{-2} and reacts with NH_3 to produce sulfate. Hanse et al. (1991) found that in a simulated cloud condition, 80% of SO_2 was oxidized to sulfate in the presence of 0.6 ppm_v NH_3 in minutes scale (less than 5 minutes), and the sulfate formation was not significant when NH_3 was not present or the water was in the gas phase. NH_3 acts as a catalyst in the oxidation of SO_2 in liquid phase.

Reactions of H_2SO_4 with NH_3 are also different in gas and liquid phase. In gas phase, the products are also different depending on the stoichiometric ratio of the two reactants, varying from NH_4HSO_4 to $(NH_4)_3H(SO_4)_2$ and $(NH_4)_2SO_4$.(eq. 1.4, eq. 1.5, eq. 1.6, respectively, Renard et al, 2004)

$$NH_3 + H_2SO_4 \leftrightarrow NH_4HSO_4 \quad \text{(Eq. 1.4)}$$

$$3NH_3 + 2H_2SO_4 \leftrightarrow (NH_4)_3H(SO_4)_2 \quad \text{(Eq. 1.5)}$$

$$2NH_3 + H_2SO_4 \leftrightarrow (NH_4)_2SO_4 \quad \text{(Eq. 1.6)}$$

Although reactions are reversible, $(NH_4)_2SO_4$ is very stable and is one of the main component of $PM_{2.5}$ generated from NH_3 atmospheric chemistry (Behera et al., 2013). In liquid phase, H_2SO_4 forms from the oxidation of dissolved SO_2, and reacts with NH_3 to form NH_4HSO_4 and $(NH_4)_2SO_4$ (Behera et al., 2013).

Other than H_2SO_4, NH_3 can also react with HNO_3 and HCl, but the affinity of H_2SO_4 with NH_3 is much stronger than the other two acids (Behera et al., 2013). So reaction first takes place between NH_3 and H_2SO_4. Excess NH_3 then reacts with HNO_3 and HCl. These small particles can cause a series of problems:

(i) *Health effects*. Brook et al. (2003) reviewed air pollution studies and confirmed the positive correlation between $PM_{2.5}$ pollution and health effects. They pointed out that sensitive people with senior age, pre-existing vascular disease and diabetes mellitus were more vulnerable to such pollution. Pope et al. found that 10 $\mu g/m^3$ decrease of $PM_{2.5}$ would result in 0.61±0.20 year increase of life expectancy in the United States (Pope et al., 2009), while each 10 $\mu g/m^3$ increase of $PM_{2.5}$ would result in about a 4%, 6%, and 8% increased risk of all-cause, cardiopulmonary, and lung cancer mortality, respectively (Pope et al., 2002). Brunekreef et al. (2005) studied the health effects of coarse Particulate Matter (PM_{10}, particles with diameter less than or equal to 10 μm) and $PM_{2.5}$ and suggested regulating coarse particles separately from.

(ii) *Radiative effects*. Radiative effects of particles include combined scattering and absorption of radiative energy, which is called direct effect, and affecting cloud formation and properties by serving as cloud condensation nuclei, which is called indirect effect (Denman et al., 2007). Scattering happens in the form of reflection, refraction and diffraction (Jacob, 1999), while absorption transforms the incoming light into other forms of energy like heat or chemical reactions

and/or emission of the light with a different wave length. Visibility degradation occurs mainly due to direct radiative effect of particles, especially $PM_{2.5}$. Yu et al. (2016) investigated the correlation between visibility degradation and $PM_{2.5}$ concentrations at different relative humidity conditions in Nanjing, China. They found that visibility was exponentially decreased when relative humidity was smaller than 80%, and maintained low values when relative humidity was larger than 80%, even in the presence of small $PM_{2.5}$ concentrations, suggesting that hygroscopic growth of PM2.5 was more responsible for visibility degradation. Yu et al. also quantified the contribution of different species in PM2.5 for visibility degradation, with the top 3 being organic matter, ammonium sulfate and ammonium nitrate.

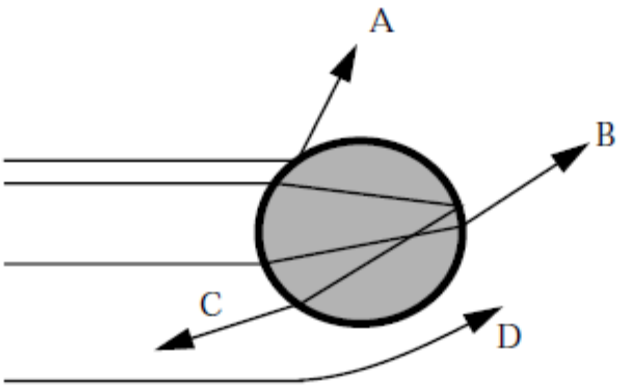

Figure 1.4 Scattering of light in 4 forms: reflection (A), refraction (B), refraction and internal reflection (C), and diffraction (D) from Jacob, 1999.

1.1.2.2 Eutrophication

Nutrients in the form of fertilization are essential for plant growth, but excessive fertilization can be harmful. Deposition of ammonium and ammonia into aquatic systems can exacerbate algal blooms, a phenomenon usually called eutrophication (U.S. EPA, 2011). Algae accumulation on the surface of aquatic system can block the sunlight away from vegetation in the submarine area, which is important habitat and food source for aquatic organisms. Dissolved

oxygen in water is quickly consumed by algae causing death of other aquatic organisms. Eutrophication can largely decrease local biological diversity and lead to degradation of water quality (Erisman et al., 2013).

1.1.2.3 Acid Rain and Soil Acidification

Natural rain has a slight acid pH range from 5 to 7 due to the dissolution of atmospheric CO_2 into rain (Jacob, 1999) (eq. 1.7, eq. 1.8) and other natural acids, like nitric acid (HNO_3), the oxidation of NO_x from lightning, and H_2SO_4, the oxidation of sulfur gases (SO_2) from volcano eruptions or the biosphere (Jacob, 1999). The term acid rain signifies rainwater with pH less than 5, which can be achieved through oxidation of excess SO_2 and NO_x from fossil fuel combustion.

$$CO_2 + H_2O \leftrightarrow CO_2 \cdot H_2O \leftrightarrow HCO_3^- + H^+ \quad \text{(Eq. 1.7)}$$

$$HCO_3^- \leftrightarrow CO_3^{2-} + H^+ \quad \text{(Eq. 1.8)}$$

Consequently, soil acidification happens when acid rain is deposited from the atmosphere. In addition, deposition of NH_x contributes soil acidification. Ammonia that reaches the soil surface, reacts with soil water in the soil and is converted into ammonium (NH_4^+). The ammonium in the soil disassociates or is nitrified into nitrite (NO_2^-) or nitrate (NO_3^-) by nitrifying bacteria, releasing H+ ions into the soil that can lead to the formation of an acidic soil environment (Eq. 1.9, Eq. 1.10). Soil acidification can result in loss of nutrient cations like calcium and potassium because the leaching is enhanced by acids (Smil, 1999).

$$2\,NH_4^+ + 3\,O_2 \xrightarrow{Nitrosomonas} 2\,NO_2^- + 2\,H_2O + 4\,H^+ \quad \text{(Eq. 1.9)}$$

$$NO_2^- + O_2 \xrightarrow{Nitrobacter} 2\,NO_3^- \quad \text{(Eq. 1.10)}$$

1.1.3 Air Quality Modeling and Uncertainty of Ammonia Emission Input

Air Quality Models (AQMs) are numerical tools that simulate physical and chemical processes of the transport and reaction of the pollutants in the atmosphere (U.S. EPA, SCRAM,

2016). Generally speaking, there are three kinds of AQM: dispersion models, receptor models and chemical transport models (CTM).

(i) Dispersion models simulate the transport of pollutants during a period of time using models like the Gaussian plume model (U.S. EPA, SCRAM, 2016). These models are very useful for determining whether the pollutant concentrations exceed the National Ambient Air Quality Standards, after permitting a new emission source, like a power plant. They perform better for inert pollutants in local to regional scales because such models typically do not include chemical mechanisms.

(ii) Receptor models use measurement data at both sources and receptors (usually from air quality monitoring stations) to calculate contribution of each source to the receptor. The most common receptor model is Chemical Mass Balance (CMB) model. Receptor models were adopted by U.S. EPA for source apportionment (Watson, 1979; Coulter, 2004).

(iii) CTMs are 3-dimensional complex models that can calculate the concentration of pollutants and deposition by numerically simulating both chemical and physical processes in the atmosphere (U.S. EPA, SCRAM, 2016). Emission inventories and meteorological data are needed as inputs for CTMs. CTMs have been used for simulating the concentrations of ozone, PM and wet deposition. Two well-known regional scale CTMs are the Community Multi-scale Air Quality (CMAQ) (Byun and Ching, 1999) and the Comprehensive Air quality Model with extensions (CAMx) (Environ, 2014).

AQMs are useful in supporting policy and evaluating implementation of legislation. However, the accuracy of model predictions, is constrained by the limited understanding of the atmospheric processes and chemical reactions in the atmosphere and the uncertain inputs of

meteorological data and emissions. This is especially true for NH_3 emissions from fertilizer application due to the fugitive nature of this source and the lack of data on spatial and temporal fertilizer management (Gilliland et al., 2006). Beusen et al. (2008) estimated the global NH_3 emissions from fertilized systems to be 10–12 Tg NH_3-N per year (10% and 90% percentile range). Balasubramanian et al. (2015) developed a new method to estimate spatial and temporal distribution of NH_3 emissions at 4 km resolution in Midwest USA and found the difference in each cell varied from -10% to 120% compared with commonly used method. Modeling studies using CTMs like CMAQ and CAMx also suggest the need for accurate NH_3 emission inputs to improve model predictions of secondary PM concentrations (Appel et al., 2011; Baker et al., 2010).

1.2 Weather Research and Forecasting (WRF) Model

1.2.1 Overview

As discussed earlier, meteorological data are needed as inputs into CTMs like CAMx or CMAQ, and this is usually done by using a prognostic Numerical Weather Prediction (NWP) model. NWP models forecast weather state in the future by considering current weather observations. The forecast is the result of solving numerically, in a three-dimension grid, the governing partial differential equations that are derived from considering conservation of momentum and mass, the continuity equation, the equation of state and the first and second law of thermodynamics (Lynch, 2008; Jacob, 1999). Currently, there are many NWP models differing in spatial scale (global or regional), temporal scale (short-term like days or long-term like months or years), purpose (operational or research) and spatial resolution (coarse domain larger than 10 km or fine domain smaller than 10 km). NOAA's National Operational Model Archive and Distribution System maintains several NWP model output data and input data for assimilation

including Global Forecast System, North American Mesoscale and Rapid Update Cycle (NOAA, 2016).

In the context of coupled modeling between Chemical Transport Models and NWP models, the Fifth-Generation Pennsylvania State University/National Center for Atmospheric Research Mesoscale Model (MM5) (Grell et al., 1994) and the Weather Research and Forecasting (WRF) model - Advanced Research WRF (WRF-ARW) (Skamarock et al., 2008) are the two most commonly used models to provide meteorological inputs for CTMs. Both of them are recommended by CAMx and CMAQ developers (UNC, 2012; Environ, 2014). The reason why only a few NWP models are compatible with CTMs is that different models have different requirements for input data, and it is almost impossible to have a universal interface program to process the NWP data into the format that CTMs require given various formats of NWP output data. Appel et al. (2010) compared performance of CMAQ for the eastern United States in January and August, with meteorological inputs from both WRF and MM5 models. The WRF-CMAQ was found to produce better performance for particulate sulfate, similar performance for nitrate as well as wet deposition, and a little worse performance for ozone, nitric acid, total carbon and total fine particulate mass compared with the MM5-CMAQ results in January, and generally underperformed in August. Wilmot et al. (2014) focused on comparing meteorological parameters between WRF and MM5 in southeastern Texas coastal region with 2 4-day runs and found that WRF gave better prediction on energy budget and temperature, while MM5 was better on water vapor mixing ratio, wind speed, wind direction and planetary boundary layer heights. Awan et al. (2011) examined the parameterization-induced error between the two models in European alpine mountains in a one-year run and WRF consistently performed better in temperature prediction than MM5. U.S. EPA (2014) suggests use of WRF over MM5 because MM5 is no longer updated and supported while WRF was developed and is maintained through a partnership among the National Center for Atmospheric Research's (NCAR), the National

Oceanic and Atmospheric Administration's (NOAA), the National Centers for Environmental Prediction (NCEP) and Earth System Research Laboratory (ESRL). WRF has a live community with many users and developers around the world, and it is designed as a next-generation mesoscale NWP system based on MM5.

WRF has two dynamic cores: the Advanced Research WRF (ARW) for research application and the Non-hydrostatic Mesoscale Model (NMM) for operational application. WRF-ARW provides advanced options in physics, numeric, and data assimilation, while WRF-NMM offers more flexible and computationally-efficient framework in operational forecasting. Yu et al. (2012a, 2012b) evaluated CMAQ performance over eastern United States with WRF-NMM and WRF-ARW as meteorological inputs. Both provided reasonable results compared with observational data, and both cores had their own advantages and disadvantages when looking into specific variables.

With regard to model evaluation, Emery et al. (2001) did extensive research on weather model performance evaluation for two Texas ozone episodes on MM5. The benchmark values suggested by Emery et al. are often referenced as a quantitative comparison to previous works in WRF. These benchmark values include temperature, wind speed, wind direction and humidity, and are adopted in this thesis. Detailed explanation are given in the methods section.

As to the choice of these two cores, both user's guides of CMAQ and CAMx only mention WRF-ARW as the default model to provide meteorological inputs (UNC, 2012; Environ, 2014). Converters like WRFCAMx (for CAMx from CAMx support software) and MCIP (Meteorology-Chemistry Interface Processor, for CMAQ from Community Modeling and Analysis System) have been developed to convert WRF-ARW output to input for CTMs, respectively. In this thesis, the focus is on WRF-ARW.

1.2.2 Choice of the Horizontal Resolution

Domain is defined as the grid cells that are overlaid over the geographical domain area of interest for air quality modeling. Since the WRF-ARW domain is created on a 3D scale, the concept of resolution includes both horizontal direction, the individual grid cell size (spacing), and vertical direction, and the number of vertical levels. In WRF, the vertical levels are defined by the highest input pressure level (default to be 5000 Pa), the number of vertical levels, and a series of fractions from 0 to 1 indicating each level. WRF also accepts the number of levels. In that case, WRF itself calculates a set of fractions with thinner layers at the bottom and thicker layers at the top (Wang et al., 2016). Most often researchers choose 30 vertical levels. Aligo et al. (2009) designed 7 configurations of vertical resolution to investigate the impact of vertical resolution on Midwest summer precipitation simulation, and found that a refined vertical grid resolution did not result in an improved simulation skill. But the simulation skill improved when resolution of above the melting level (height when temperature becomes more than 0 °C) was increased.

As to the horizontal resolution, there is a clear trend of increasing the horizontal resolution in the NCEP operational weather models, from 381 km of the National Meteorological Center barotropic model in the middle of last century, to the 190.5 km of the Limited-area Fine-mesh Model, and to the current 12 km of the Eta Model (Mass et al., 2002; Roebber et al., 2004). However, whether fine horizontal resolution (generally less than 10 km) will result in improved weather model simulation skill is still unclear. Li et al. (2014) reported that a WRF run with 3 km resolution takes 125 times more computing time than that with 15 km, while not outperforming in terms of precipitation simulation skill in the southeastern United States. Mass et al. (2002) found a clear model improvement from 36 km to 12 km when simulating wind direction, temperature, and precipitation, but little difference when increasing resolution from 12 km to 4 km. This point of diminishing return is different between northwestern and eastern United States because details

like ridges or valleys in complicated terrain need finer resolution to capture. However, Mass et al. (2002) pointed out that the traditional evaluation approach using point observation at fixed locations, which is greatly influenced by spatial and temporal error, might not be a fair way for evaluating fine resolution model results. Instead, they suggest that comparisons could be extended to include temporal or spatial shifting of model fields to verify model structures for subsequent days or neighboring areas.

Besides weather model simulation skill, Queen et al. (2008) used the MM5-CMAQ model with 4 km, 12 km, and 36 km over North Carolina for August and December 2012 and found no clear pattern of differences in model performance with these horizontal resolutions. The model with 36 km resolution produced the best simulation for NH_4^+ and NO_3^- in December, while model with 12 km resolution performed best for NH_4^+ and SO_4^{2-} in August and with 4 km resolution for NO_3^- in August and SO_4^{2-} in December.

1.2.3 WRF Physics Overview

WRF includes many options (the word "scheme" is also used when referring to a specific option) for describing physics in the modelled domain, as shown in Table 1.1 (Skamarock et al., 2008).

Table 1.1 Summary of WRF Physics categories (Skamarock et al., 2008).

Physics category	**Definition**	**Examples of the physics options**
Microphysics	Explicitly resolved water vapor, cloud, and precipitation processes	Kessler scheme, Purdue Lin scheme, WRF Single-Moment 3-class (WSM3) scheme, WSM6 scheme, Thompson et al. scheme
Cumulus parameterization	Sub-grid-scale effects of convective and/or shallow clouds	Kain-Fritsch scheme, Betts-Miller-Janjic scheme, Grell-Devenyi ensemble scheme, Grell-3 scheme
Surface Layer	Calculation of friction velocities and exchange coefficients that enable the calculation of surface heat and moisture fluxes by the land-surface models and surface stress in the planetary boundary layer scheme	MM5, Eta, Pleim-Xiu
Land Surface Model	Provides heat and moisture fluxes over land points and sea-ice points with atmospheric information from the surface layer scheme, radiative forcing from the radiation scheme, and precipitation forcing from the microphysics and convective schemes, together with internal information on the land's state variables and land-surface properties	Thermal diffusion, Noah LSM, Rapid Update Cycle (RUC) Model LSM, Pleim-Xiu LSM
Planetary Boundary Layer (PBL)	Vertical sub-grid-scale fluxes due to eddy transports in the whole atmospheric column	Yonsei University (YSU) PBL, Mellor-Yamada-Janjic (MYJ) PBL, Asymmetrical Convective Model version 2 (ACM2) PBL
Atmospheric Radiation	Atmospheric heating due to radiative flux divergence and surface downward longwave and shortwave radiation for the ground heat budget	Rapid Radiative Transfer Model (RRTM) Longwave, RRTMg Longwave/shortwave, MM5 (Dudhia) Shortwave, Goddard Shortwave

The interactions of each physics category is shown in Figure 1.5 (Dudhia, 2012). The flow chart indicates that these physics categories are not independent of each other. When discussing about physics interactions, surface layer and land surface model were often grouped together as surface physics (Skamarock et al., 2008; Dudhia, 2012). Skamarock et al. (2008) emphasized that all the physics categories had interactions with the surface physics in some way. Dudhia (2012) also discussed about the close interactions between surface physics and planetary

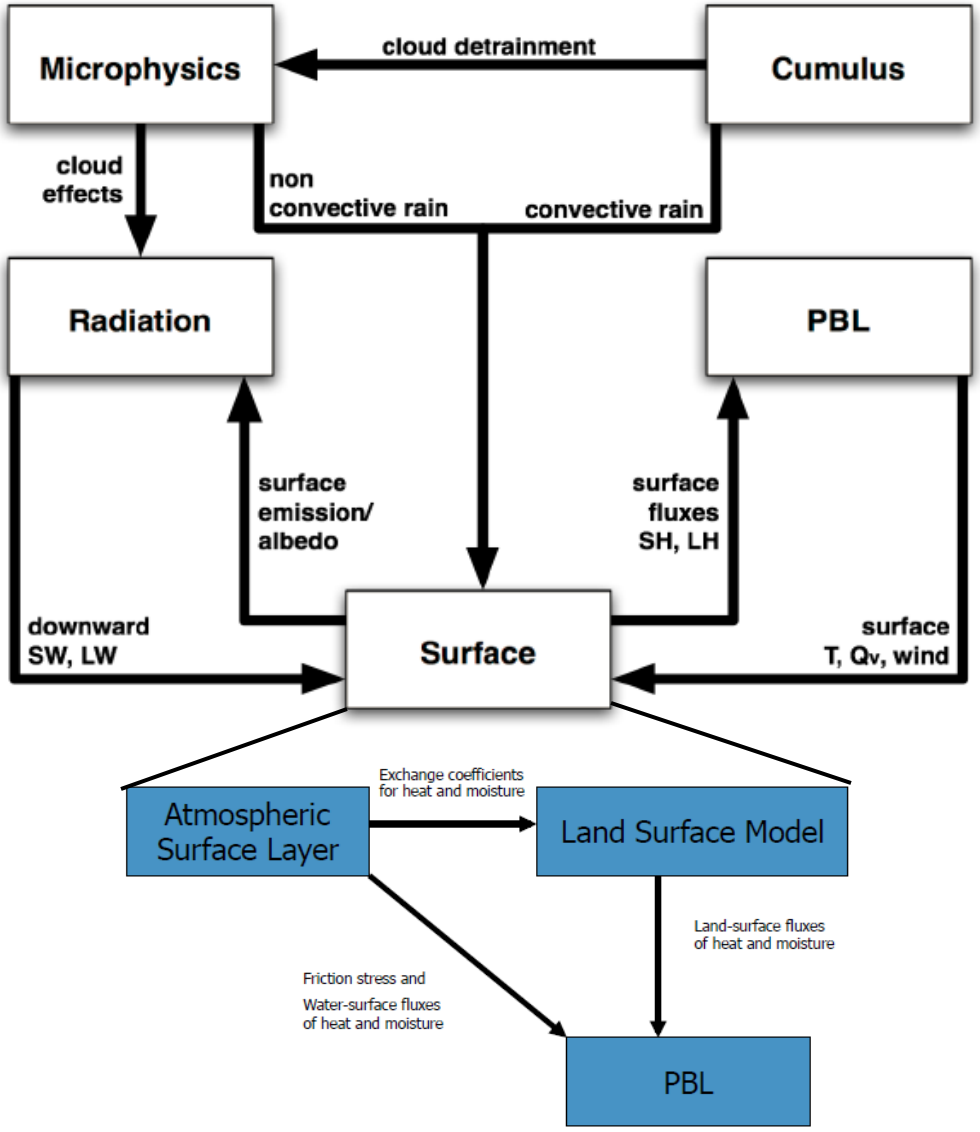

Figure 1.5 Interactions of each physics category in WRF. Surface physics includes atmospheric surface layer and land surface model (blue boxes) (Dudhia, 2012).

boundary layer. In practice, there are 7 lines in WRF namelist (the WRF ARW configuration file) describing WRF physics because radiation is split into shortwave and longwave radiation, and land surface model and surface layer have separate parameters.

Researches have demonstrated the influence of different choices of these physics schemes on the performance of WRF predictions. Awan et al. (2011) conducted 29 one-year runs on European alpine region and confirmed that significant improvement of model simulation skill can be obtained by choosing a suitable model configuration. Such configuration can be achieved by conducting a series of WRF run with different combination of physics schemes, and comparing the output with measured meteorological parameters. The approach followed in this thesis is elaborated in the methods section.

1.3 Motivation, Research Objectives, and Significances

1.3.1 Motivation

The research presented in this thesis is part of a broader research effort to accurately quantify ammonia emissions from fertilizer usage and use of the improved inventory as input to CAMx for improved predictions of regional air quality modeling. The research presented in this thesis is motivated by the need of meteorological data as inputs to CAMx as well as to the emission processor SMOKE (Sparse Matrix Operator Kernel Emissions) model (CMAS, 2015).

1.3.2 Research Objectives and Significance

- Determine the impact of different WRF-ARW options (including physics, nesting, horizontal resolution and spin-up time) on WRF-ARW output, for the Midwest USA domain.

- Investigate the performance of WRF-ARW at two spatial resolutions (12 km × 12 km and 4 km × 4 km grid size). Wise spatial resolution choice can save a lot of computational time while preserving accuracy of the simulation.

The unique contribution of this thesis is to explore the optimum physics configuration for WRF run over Midwest USA, which has only been done in this area by few researchers (for example, Brown et al., 2007, 2011). In this research, the optimum physics configuration was obtained for May 2011 and was evaluated for October 2011 to examine its performance over different seasons. The two months of May and October were chosen because they are months within the typical planting and harvesting periods for fertilized crops, in Midwest USA. Finding optimum physics configurations for WRF is important because reliable predictions of pollutant concentrations in CTMs rely on accurate input of weather variables simulations in WRF output, and such studies in Midwest USA will be beneficial for modelling studies that require weather data as input. Methods presented in this thesis can also be reference in future regional sensitivity analysis studies.

CHAPTER 2: METHODS

2.1 Model Season, Domain, and Configuration

The WRF model (version 3.5.1) simulation was conducted from May 4, 00 h UTC to May 10, 00 h UTC in 2011, with two spatial domains over the Midwest USA (Figure 2.1), a 2-day spin-up time and 1 hour output time interval to determine the optimal physics configuration for the specific geographical domain.. One-way nesting (no feedback from nested domain to coarse domain) was used at a grid size of 4 km for a nested domain (181 rows x 253 columns) covering Illinois and adjacent states and a coarse domain of 12 km grid size (369 rows x 481 columns) covering North America (Figure 2.1). 30 Eta Levels were used in the vertical direction, interpolated by WRF's default algorithm. Lambert Conformal Projection was used when creating domains in WRF. Both nesting and spin-up time choices were explored with different configurations and results are discussed in the results chapter.

Once optimum parameters were determined for the May period, WRF performance was then tested for the time period from October 25, 00 h UTC to October 31, 00 h UTC. October was selected to investigate whether the optimum physics combination can be used throughout the

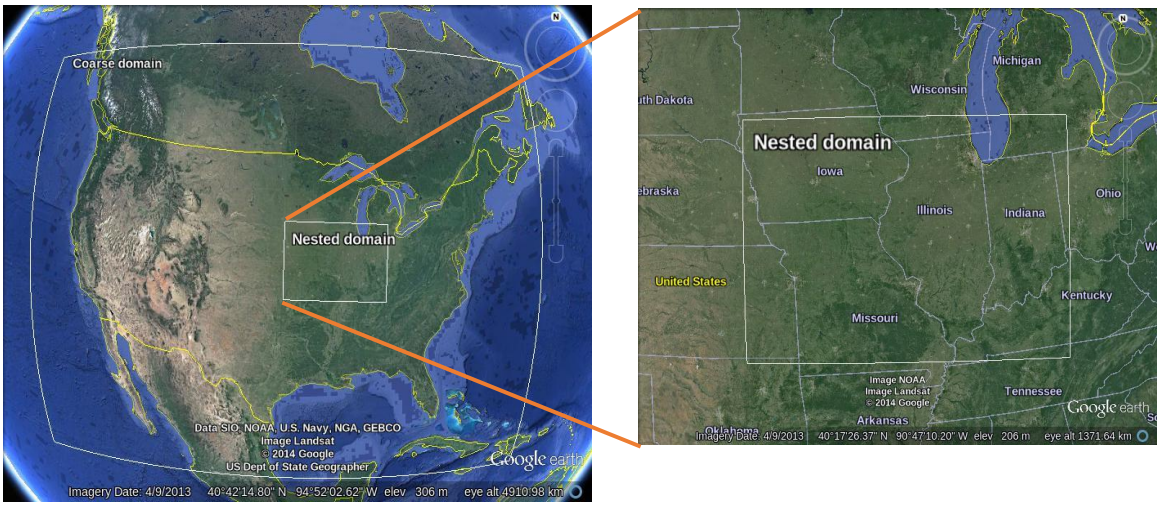

Figure 2.1 WRF coarse domain and nested domain (Lambert Conformal Projection).

whole year. Simulation periods in spring and fall were chosen based on the planting and harvesting time of corn and soybean, at local farmlands, in 2011.

Initial and boundary conditions for WRF simulations were driven by the 12-km North American Model (NAM) data from National Operational Model Archive & Distribution System, with 6-hour temporal resolution (NOAA, 2016). The terrain input data were obtained from the WRF official website (UCAR, 2016).

2.2 Sensitivity Analysis Design to Obtain the Optimum Physics Configuration

A sensitivity analysis is a method to test the response of the model output to the perturbation of inputs (Pannell et al., 1997). Sensitivity analysis can be used in many areas, including decision making, model development and model evaluation. As to how the inputs are chosen, there are many approaches. One straightforward way is to vary one input (e.g., vary by 10%) at a time and keep all the other inputs the same (Pannell et al., 1997).

In this thesis, the purpose of the sensitivity analysis was to investigate what is the optimum WRF physics configuration for a given season and domain by varying the physics options and then comparing model predictions with measurement data. As discussed in the introduction, WRF has several physics categories: cumulus, surface layer, microphysics, land surface model, planetary boundary layer, and longwave/shortwave radiation. In each physics category there are several physics schemes to choose. Each scheme is an algorithm to represent the physics process mathematically. However, there is no apparent perfect model that can perfectly represent the real world, and each scheme has its own strengths and weaknesses. It is very hard to determine the best physics schemes by just looking into the details of each scheme. According to U.S. EPA's "Modeling Guidance for Demonstrating Attainment of Air Quality Goals":

"In many situations, the "optimal" configuration cannot be determined without performing an initial series of sensitivity tests which consider various combinations of physics options over specific time periods and regions. "(U.S. EPA, 2014)

"Over specific time periods and regions" indicates that there is no universal physics scheme that can be applied to all times and everywhere. That is why different researchers conduct their own sensitivity analysis for their specific use.

Usually researchers conduct sensitivity analyses for WRF in three steps, as suggested by U.S. EPA (U.S. EPA, 2014): creating a series of WRF runs, run WRF according to their plan, and compare the results with observational data. Researchers have developed their own approaches as to how to create their series of WRF runs and their design table. Most researchers (Appel et al., 2010; Zhang et al., 2012; Pérez et al., 2014; Remesan et al., 2014) first chose physics categories that are of interest, then picked several (e.g., average of 10 cases) combinations of the physics options. Some researchers (Borge et al., 2008; Nobel et al., 2014) tried to perform a more thorough sensitivity analysis and chose more physics categories and physics schemes. Tables 2.1, 2.2, 2.3 and 2.4 show design tables used by different researchers. Generally speaking, a design table records the physics options of each physics category in each run (also called case or scenario), so a typical design table usually has a list of physics options and case names as reference. Sometimes a baseline case is determined and all the other cases are compared with the baseline (Table 2.2), but that is not always done, as shown in other design tables. Also, sensitivity analysis in WRF is not constrained in physics option. Zhang et al (2012) investigated impact of different grid resolutions on the WRF (Table 2.1), and Borge et al. (2008) added four dimensional data assimilation option in the design table (Table 2.3).

Creating a design table and choosing combinations of physics options for the sensitivity analysis is not trivial. In WRF there are seven available physics categories (radiation is split into shortwave and longwave radiation in the WRF configuration file) and each category has more

than 10 schemes. Because users need to make a decision about what to choose in all the physics categories, the possible combinations of physics options are of 10^7 order of magnitude due to the multiplication principle. It would be very time consuming and computationally expensive to run all these combinations. Zhang et al. (2012) and Pérez et al. (2014) ignored the multiplication principle and chose cases of interest in a straightforward manner (Table 2.1, Table 2.2). Borge et al. (2008) came up with a more thorough design table listing more physics options of interest in each physics category, and then changed one scheme at a time while keeping the others the same (Table 2.3). Noble et al. (2014) followed the multiplication principle but reduce the number of physics categories and physics options in different physics categories to make the sensitivity analysis computationally affordable, ending up with 64 cases ($64 = 2 \times 4 \times 4 \times 2$) in total (Table 2.4).

Table 2.1 Design table for the sensitivity analysis from Zhang et al. (2012).

RUN SET	RUN NAME	RESOLUTION	MICRO PHYSICS	LSM	CUMULUS	SHORT WAVE	LONG WAVE
BASELINE	Base	1" X 1"	WSM3	NOAH	KF	Goddard	CAM
SENSITIVITY	CMP1	1" X 1"	WSM6	NOAH	KF	Goddard	CAM
	CMP2	1" X 1"	Purdue Lin	NOAH	KF	Goddard	CAM
	LSM	1" X 1"	WSM3	Thermal	KF	Goddard	CAM
	RAD1	1" X 1"	WSM3	NOAH	KF	Dudhia	CAM
	RAD2	1" X 1"	WSM3	NOAH	KF	CAM	RRTM
	RAD3	1" X 1"	WSM3	NOAH	KF	CAM	CAM
	CCP	1" X 1"	WSM3	NOAH	GD	Goddard	CAM
	OPT	1" X 1"	WSM6	Thermal	GD	CAM	RRTM
	Low-Res	4" X 5"	WSM3	NOAH	KF	Goddard	CAM

Table 2.2 Design table for the sensitivity analysis from Pérez et al. (2014).

SCENARIO	MP	PBL	LSM	CP	RADIATION
CTRL	WDM6	YSU	Noah	KF	CAM3
MP-THOM	THOM	YSU	Noah	KF	CAM3
PBL-MYJ	WDM6	MYJ	Noah	KF	CAM3
CU-TI	WDM6	YSU	Noah	TI	CAM3
LSM-PX	WDM6	YSU	PX	KF	CAM3
DSST	WDM6	YSU	Noah	KF	CAM3

Table 2.3 Design table for the sensitivity analysis from Borge et al. (2008).

PARAMETER	OPTION
PBL – SURFACE LAYER	Medium Range Forecast Model (MRF) PBL – Similarity theory (MM5)
	Yonsei University (YU) PBL – Similarity theory (Eta)
	Mellor-Yamada-Janjic (MYJ) PBL – Similarity theory (MM5)
MICRO PHYSICS	WSM5 scheme
	Purdue Lin scheme
	WSM6 scheme
	Eta Grid-scale Cloud and Precipitation (2001) scheme
LAND-SURFACE MODEL	5-layer thermal diffusion
	Noah LSM
	Rapid Update Cycle (RUC) Model LSM
SEA SURFACE TEMPERATURE	Time-varying
	Constant
RADIATION SCHEME	Longwave ---- Rapid Radiative Transfer Model (RRTM)
	Longwave ---- Eta Geophysical Fluid Dynamics Laboratory (GFDL) Community Atmospheric Model (CAM)
	Shortwave ---- Eta Geophysical Fluid Dynamics Laboratory (GFDL) MM5 (Dudhia)
	Shortwave ---- Goddard
FOUR-DIMENSIONAL DATA ASSIMILATION (FDDA)	Nudging ---- Analysis (grid)
	Nudging ---- Stations (observational)
	Nudging ---- Both (grid + observational)
	Without nudging

Table 2.4 Design table for the sensitivity analysis from Noble et al. (2014).

WRF EXPT	CUMULUS	PBL	LSM	RADIATION
1	KF	YU	thermal	RRTMg
2	KF	YU	Noah	RRTMg
3	KF	YU	RUC	RRTMg
4	KF	YU	Pleim-Xiu	RRTMg
5	KF	MYJ	thermal	RRTMg
6	KF	MYJ	Noah	RRTMg
7	KF	MYJ	RUC	RRTMg
8	KF	MYJ	Pleim-Xiu	RRTMg
9	KF	ACM2	thermal	RRTMg
10	KF	ACM2	Noah	RRTMg
11	KF	ACM2	RUC	RRTMg
12	KF	ACM2	Pleim-Xiu	RRTMg
13	KF	MN	thermal	RRTMg
14	KF	MN	Noah	RRTMg
15	KF	MN	RUC	RRTMg
16	KF	MN	Pleim-Xiu	RRTMg
17	GD	YU	thermal	RRTMg
18	GD	YU	Noah	RRTMg
19	GD	YU	RUC	RRTMg
20	GD	YU	Pleim-Xiu	RRTMg
21	GD	MYJ	thermal	RRTMg
22	GD	MYJ	Noah	RRTMg
23	GD	MYJ	RUC	RRTMg
24	GD	MYJ	Pleim-Xiu	RRTMg
25	GD	ACM2	thermal	RRTMg
26	GD	ACM2	Noah	RRTMg
27	GD	ACM2	RUC	RRTMg
28	GD	ACM2	Pleim-Xiu	RRTMg
29	GD	MN	thermal	RRTMg
30	GD	MN	Noah	RRTMg
31	GD	MN	RUC	RRTMg
33	KF	YU	thermal	CM
34	KF	YU	Noah	CM
35	KF	YU	RUC	CM
36	KF	YU	Pleim-Xiu	CM
37	KF	MYJ	thermal	CM
38	KF	MYJ	Noah	CM
39	KF	MYJ	RUC	CM
40	KF	MYJ	Pleim-Xiu	CM
41	KF	ACM2	thermal	CM

Table 2.4 (cont.) Design table for the sensitivity analysis from Noble et al. (2014)

WRF EXPT	CUMULUS	PBL	LSM	RADIATION
42	KF	ACM2	Noah	CM
43	KF	ACM2	RUC	CM
44	KF	ACM2	Pleim-Xiu	CM
45	KF	MN	thermal	CM
46	KF	MN	Noah	CM
47	KF	MN	RUC	CM
48	KF	MN	Pleim-Xiu	CM
49	GD	YU	thermal	CM
50	GD	YU	Noah	CM
51	GD	YU	RUC	CM
52	GD	YU	Pleim-Xiu	CM
53	GD	MYJ	thermal	CM
54	GD	MYJ	Noah	CM
55	GD	MYJ	RUC	CM
56	GD	MYJ	Pleim-Xiu	CM
57	GD	ACM2	thermal	CM
58	GD	ACM2	Noah	CM
59	GD	ACM2	RUC	CM
60	GD	ACM2	Pleim-Xiu	CM
61	GD	MN	thermal	CM
62	GD	MN	Noah	CM
63	GD	MN	RUC	CM
64	GD	MN	Pleim-Xiu	CM

Methods in this thesis were mainly borrowed from Borge et al. (2008), with a slight modification. Borge et al. fixed their base case of the physics configuration, and compared all the other runs with the baseline case. In this thesis, there was no global baseline case. Instead, a starting case was selected based on a previous study (Appel et al., 2011). Sensitivity analysis was divided into several stages. One physics category was examined at each stage. The best option for each physics category was selected by changing one scheme at a time and comparing the WRF

output with the observational data, while keeping schemes in other physics categories unchanged. When one physics category (stage) was finished (e.g., microphysics), the optimum option resulting from that stage was used into the remaining stages, acting as a local baseline case that was updated in each stage. After iterative testing of all the stages, the optimum combination of choices in each physics category was obtained. Table 2.5 shows the design table of the sensitivity analysis in this thesis, and Figure 2.2 shows the flowchart of this method.

In practice, surface physics (land surface model and planetary boundary layer), as well as radiation (longwave and shortwave) were grouped together because they were closely related with each other, as mentioned in the introduction. One exception about changing only one scheme at a time was the Zhang-Mc scheme in cumulus and the MYJ scheme in planetary boundary layer. These two schemes must be used together. The Eta scheme in surface layer can also only be used with the MYJ scheme in planetary boundary layer according to WRF users' guide (Wang et al., 2016).

Table 2.5 Physics options design table for the sensitivity analysis. Red boxes group WRF runs in the same stage.

WRF run	Micro physics	Longwave Radiation	Shortwave Radiation	Surface Layer	Land Surface Model	Planetary Boundary Layer	Cumulus
1	WSM6	RRTM	Dudhia	Monin-Obukhov	Pleim-Xiu	ACM2	KF
2	WSM6	RRTM	Dudhia	Monin-Obukhov	Pleim-Xiu	ACM2	GF
3	WSM6	RRTM	Dudhia	Eta	Pleim-Xiu	MYJ	Zhang-Mc
4	WSM6	RRTM	Dudhia	Monin-Obukhov	Pleim-Xiu	ACM2	KF,turn off
5	WSM6	RRTM	Dudhia	Eta	Pleim-Xiu	MYJ	
6	WSM6	RRTM	Dudhia	Pleim-Xiu	Pleim-Xiu	ACM2	
7	Lin	RRTM	Dudhia		Pleim-Xiu	ACM2	
8	Eta	RRTM	Dudhia		Pleim-Xiu	ACM2	
9	Thompson	RRTM	Dudhia		Pleim-Xiu	ACM2	
10		RRTM	Dudhia		Noah	ACM2	
11		RRTM	Dudhia		Noah	YSU	
12		RRTM	Dudhia	Eta	Noah	MYJ	
13		RRTM	Dudhia		Pleim-Xiu	YSU	
14		RRTM	Dudhia	Eta	Pleim-Xiu	MYJ	
15		RRTMg	Dudhia				
16		Goddard	Dudhia				
17		RRTMg	RRTMg				

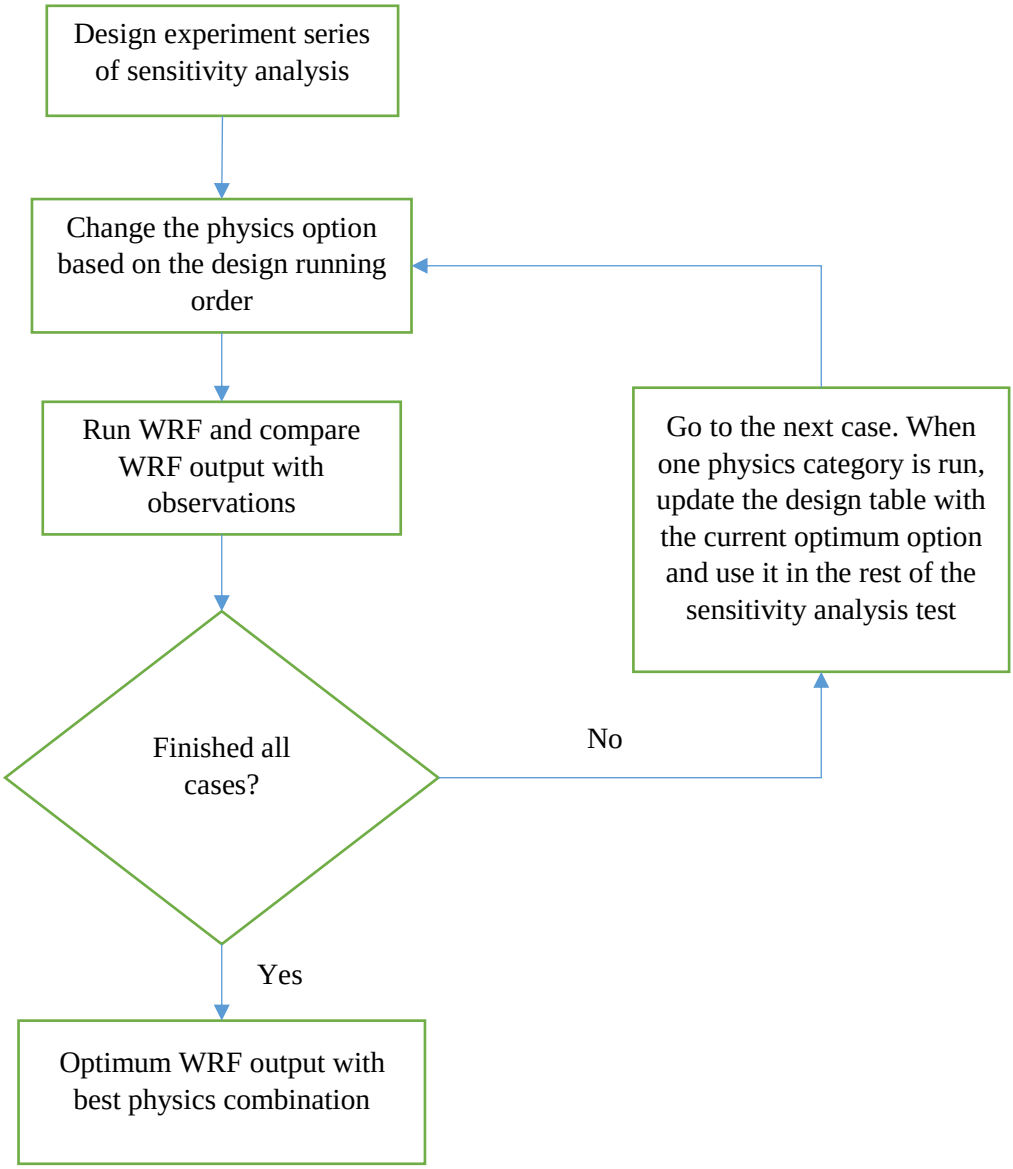

Figure 2.2 Flow chart of the sensitivity analysis method in this thesis.

2.3 Evaluation Protocol and Datasets

2.3.1 Evaluation protocol

The purpose of running WRF is to provide three dimensional (3D) meteorological inputs to CAMx (Environ, 2014). Therefore, for evaluating the performance of WRF, we considered these outputs that are required inputs for CAMx. These are the time-variant 3D meteorological parameters of pressure (Pres), wind, temperature, humidity (specific humidity, SH; relative humidity, RH), and precipitation. Precipitation was not considered in this evaluation because there happened to be little rain (less than 0.1 inch on average from observation data) from May 6 to May 10 in 2011. Temperature was compared at 2 m (T2) above ground, and wind speed and direction at 10 m (WS10 and WDir10) above ground. There is another way to represent the wind variable by the decomposition of the horizontal wind vector, which includes the zonal wind speed towards east (UGRD) and meridional wind speed towards north (VGRD) and is adopted as the standard way to describe wind in GRIdded Binary (GRIB) data format (a World Meteorological Organization data format standard for exchanging gridded binary data). Benchmark values (Table 2.3) from MM5 (Emery et al., 2001) were considered for the following statistical terms: RMSE (Root Mean Square Error), MB (Mean Bias), GE (Gross Error), IOA (Index of Agreement), and Correlation Coefficient (CC). The formulas for these statistical terms are shown in Table 2.2. It should be noted that benchmark values are not meant to be pass/fail indicators, but as a quantitative guideline to help compare with previous studies (McNally et al., 2002). Also, wind speed in the benchmark table should not be confused with the UGRD and VGRD. However, since Emery et al. (2001) did not include UGRD and VGRD in their research, the same benchmark value of wind speed was used for UGRD and VGRD in this thesis, which is necessary but not sufficient.

Choosing the optimum case is not self-evident. Ideally, the optimum case should outperform other cases with lower RMSE, MB and GE, as well as higher IOA and CC (close to

1). However, results between different cases were often similar, and no case could achieve that goal over all five statistical terms. This is reasonable because WRF is a state-of-art weather modelling system and physics parameterization is robust enough to use in different conditions. There are still some rules when picking the optimum case in each stage. RMSE and GE weighs more over MB in terms of reliability because MB can cancel negative and positive errors in some occasions. IOA and CC are also important factors to assess the overall performance. IOA was introduced by Willmott in 1981 and is a standardized statistic term measuring the degree of model prediction error (Moriasi et al., 2007). CC is also a commonly used statistic term describing collinearity of two variables. IOA is focused on agreement while CC on correlation. For example, array [1, 2, 3] and array [4, 5, 6] have perfect correlation (CC = 1) but bad agreement (IOA ≈ 0.628).

Table 2.6 Statistical terms used for model evaluation. f_i stands for forecast data and o_i stands for observation data (Emery et al., 2001).

Statistic term	Abbreviation	Formula
Root Mean Square Error	RMSE	$\sqrt{\frac{1}{N}\sum(f_i - o_i)^2}$
Mean Bias	MB	$\frac{1}{N}\sum(f_i - o_i)$
Gross Error	GE	$\frac{1}{N}\sum\lvert f_i - o_i\rvert$
Index of Agreement	IOA	$1 - \frac{\sum(f_i - o_i)^2}{\sum(\lvert f_i - \bar{o}\rvert + \lvert o_i - \bar{o}\rvert)^2}$
Correlation Coefficient	CC	$\frac{\sum(f_i - \bar{f})(o_i - \bar{o})}{\sqrt{\sum(f_i - \bar{f})^2}\sqrt{\sum(o_i - \bar{o}_i)^2}}$

Table 2.7 Benchmark value for model evaluation (Emery et al., 2001).

Parameter	Statistic	Benchmark
Wind Speed	RMSE	< 2 m/s
	MB	< ±0.5 m/s
	IOA	≥ 0.6
Wind direction	GE	< 30°
	MB	< ±10°
Temperature	GE	< 2 K
	MB	< ± 0.5 K
	IOA	≥ 0.8
Specific humidity	GE	< 2 g/kg
	MB	< ±1 g/kg
	IOA	≥ 0.6

2.3.2 Description of Data Analysis Tool and Observational Datasets

Two evaluation tools were used in this thesis: Model Evaluation Tools (MET) (DTC, 2016) and the NCAR Command Language (NCL) (NCL, 2016). MET is a software package designed for WRF evaluation, developed by the NCAR Developmental Testbed Center (DTC). The main goal of MET is to provide state-of-the-art verification techniques and facilitate the process of evaluating models. It consists of several useful modules that can meet different verification needs, including grid-to-point (Point-Stat) and grid-to-grid (Grid-Stat) comparisons. MET also provides various converters for popular weather data formats, including the MADIS data and DS 337.0 (PrepBufr format, a format used in preparing the observational data for assimilation in NCEP). These two datasets are also suggested in the DTC MET official website at the “Observation Datasets” section and were chosen as observational data for comparison in this thesis.

NCL is an interpreted language designed for data analysis and visualization by the Computational & Information Systems Laboratory at the NCAR. The NCL provides numerous functions to directly process the WRF raw output (e.g., calculating relative humidity that is not

originally generated in the WRF output). NCL is essentially a programming language and provides more flexibilities compared with MET. NCL is officially introduced in both the WRF users' guide and WRF online tutorial. In this thesis, NCL was used to calculate the station level statistics and make time-series and scatter plots from the Water and Atmospheric Resources Monitoring network data (ISWS, 2016).

DS337.0 (NCEP, 2016a) is the NCEP ADP (Automatic Data Processing) Global Upper Air and Surface Weather Observations, which includes land surface, marine surface, radiosonde, pibal (pilot balloon) and aircraft reports from the Global Telecommunications System (GTS), profiler and US radar derived winds, SSM/I oceanic winds and TCW retrievals, and satellite wind data from the National Environmental Satellite Data and Information Service (NESDIS). Temperature at 2 m (T2, K), specific humidity (SH, g/kg), wind speed (m/s) at 10 m were extracted and compared with model outputs. UGRD and VGRD were used to represent the vector component of horizontal wind based on the GRIB convention. The temporal resolution is 6 hr.

METAR data is a subset of MADIS (Meteorological Assimilation Data Ingest System) (NCEP, 2016b) datasets for single station data. MADIS started collecting METAR data over the US on July 1, 2001 and moved to global coverage on March 13, 2006. T2, UGRD and VGRD were extracted and compared with model outputs. The temporal resolution is 1 hr.

Figure 2.3 19 weather stations in WARM Network (ISWS, 2016).

The Water and Atmospheric Resources Monitoring (WARM) Network (ISWS, 2016) in Illinois State Water Survey monitors atmospheric parameters at 19 stations all over the state of Illinois (Figure 2.3). The WARM dataset includes both daily and hourly averaged data. They are ASCII texts in tabular structure, which is easy to read in NCL. T2, RH, WS10 and WDir10 were extracted for daily comparison and the same as wells as Pres for hourly comparison with model outputs. The Bondville station was chosen for single station comparison.

CHAPTER 3: RESULTS AND DISCUSSION

As explained in the methods section, both the MET software package and NCL were used in evaluating the WRF outputs. MET accepts data in DS337.0 and METAR formats and provides aggregated statistical evaluation. NCL is even more flexible regarding input formats and facilitates use of on-site level data. Since the purpose of sensitivity analysis is to explore the optimum physics combination, the results section is organized to display results in the order of physics categories considered with both MET and NCL. The difference between these two methods are the temporal resolution and weather parameters. MET was used to compare T2, SH, UGRD and VGRD from DS337.0 (6-hour interval) and MADIS (1-hour interval), and NCL was used to compare T2, RH, WS10, Pres, and WDir10 from WARM (both daily and hourly for all the 19 Illinois stations). In addition, Bondville, Illinois, was chosen to represent single station data.

When presenting the statistics in the table, number in red and italic indicates it is out of the benchmark range, and number in bold indicates it is the best value when compared among all the possible schemes for each statistic term.

3.1 Cumulus Parameterization

In this stage, Kain-Fritsch (KF) scheme, Grell-Freitas (GF) scheme and Zhang-McFarlane (Zhang-Mc) scheme in cumulus parameterization were considered and evaluated (Table 3.1). Here “turned off” means KF scheme for coarse domain and no scheme for nested domain.

Table 3.1 Physics options design table in cumulus parameterization stage.

Physics category to test	Micro-physics	Longwave radiation	Shortwave radiation	Surface layer	Land surface model	Planetary boundary layer	Cumulus
Cumulus	WSM6	RRTM	Dudhia	Monin-Obukhov	Pleim-Xiu	ACM2	KF
	WSM6	RRTM	Dudhia	Monin-Obukhov	Pleim-Xiu	ACM2	GF
	WSM6	RRTM	Dudhia	Eta	Pleim-Xiu	MYJ	Zhang-Mc
	WSM6	RRTM	Dudhia	Monin-Obukhov	Pleim-Xiu	ACM2	KF,turn off

Table 3.2 summaries the results for the cumulus stage evaluation. The Mean Bias of temperature was about -1 K, with the exception of Zhang-MC scheme, which gave -1.7 K. All were outside the benchmark range of ±0.5K. Early in the analysis, Zhang-MC scheme was excluded due to its overall poor performance. KF, GF and turned off option were similar in nearly every statistical term, with the difference only in the third decimal point. Skamarock et al. (2008) suggested not to use the cumulus parameterizations for grid size less than 5 km because the model itself can resolve the convective eddies at such a fine scale. Therefore, “turned off” for the nested domain and KF for the coarse domain were selected in the remaining stages.

It needs to be noted that the poor performance of the Zhang-Mc scheme does not mean that this is a generally poor performing cumulus parameterization. It only shows that it does not reproduce well observations in the Midwest USA during spring season. Li et al. (2014) found Zhang-Mc to be the best scheme for Cumulus parameterization for predicting summer rainfall in the southeastern United States. These findings further support the need to conduct sensitivity analysis for different regions and seasons.

Table 3.2 Statistics from MET (data interval: DS337, 6-hour; MADIS, 1-hour) in cumulus parameterization stage.*

		T2 (K)		SH (g/kg)	UGRD (m/s)		VGRD (m/s)	
Statistic	Scheme	DS337	MADIS	DS337	DS337	MADIS	DS337	MADIS
RMSE	KF	2.42	2.14	1.34	1.61	1.57	**1.69**	**1.69**
	GF	2.40	2.13	1.32	1.61	**1.57**	1.69	1.69
	Zhang-Mc	3.07	2.63	2.38	*2.32*	*2.21*	*2.43*	*2.35*
	turned off	**2.39**	**2.13**	**1.31**	**1.61**	1.57	1.69	1.69
MB	KF	*-1.02*	*-0.84*	0.54	0.05	0.02	-0.13	-0.08
	GF	*-1.01*	*-0.83*	0.52	**0.04**	**0.02**	-0.12	-0.08
	Zhang-Mc	*-1.77*	*-1.47*	*1.42*	*-0.50*	-0.49	**-0.03**	**-0.03**
	turned off	***-1.00***	***-0.82***	**0.52**	0.05	0.03	-0.13	-0.08
GE	KF	1.87	1.71	0.91	1.21	1.19	**1.23**	**1.20**
	GF	1.85	1.70	0.90	1.22	**1.19**	1.23	1.21
	Zhang-Mc	*2.29*	*2.02*	1.66	1.63	1.59	1.60	1.56
	turned off	**1.85**	**1.70**	**0.90**	**1.21**	1.19	1.24	1.21
IOA	KF	0.97	0.97	0.94	0.94	0.94	**0.88**	**0.88**
	GF	0.97	0.97	0.95	0.94	**0.94**	0.88	0.88
	Zhang-Mc	0.94	0.95	0.85	0.90	0.90	0.80	0.81
	turned off	**0.97**	**0.97**	**0.95**	**0.94**	0.94	0.88	0.88

** red and italic: out of the benchmark range, bold: best value identified*

3.2 Surface Layer

In this stage, the Monin-Obukhov surface layer, the Eta similarities and the Pleim-Xiu surface layer in surface layer were considered. When running WRF, the choice of the surface layer is closely related to the choice of the land surface model. The Pleim-Xiu scheme in the surface layer has to be used together with the Pleim-Xiu scheme in the land surface model (Wang et al., 2016).

Table 3.3 Physics options design table in the surface layer stage.

Physics category to test	**Micro-physics**	**Longwave radiation**	**Shortwave radiation**	**Surface layer**	**Land surface model**	**Planetary boundary layer**	**Cumulus**
Surface layer	WSM6	RRTM	Dudhia	Monin-Obukhov	Pleim-Xiu	ACM2	KF,turn off
	WSM6	RRTM	Dudhia	Eta	Pleim-Xiu	MYJ	KF,turn off
	WSM6	RRTM	Dudhia	Pleim-Xiu	Pleim-Xiu	ACM2	KF,turn off

Overall the Eta scheme was found to be slightly better in predicting temperature and pressure, but much worse in wind speed (Table 3.4). Figure 3.1 shows the comparison of wind speed and wind direction between Eta and Pleim-Xiu schemes for data at Bondville. Pleim-Xiu was better in capturing the trend of wind speed (Figure 3.1c), but with a consistent underestimation. Both schemes did not capture the sudden change in wind direction observed close to 90 hr since the simulation start time (Figure 3.1a, Figure 3.1c). This period of time also corresponded to a big underestimation (about 4 m/s difference) of the gust in the wind speed plot, which explains the abnormal statistics of the wind component in the WRF simulation at Bondville (Table 3.5).

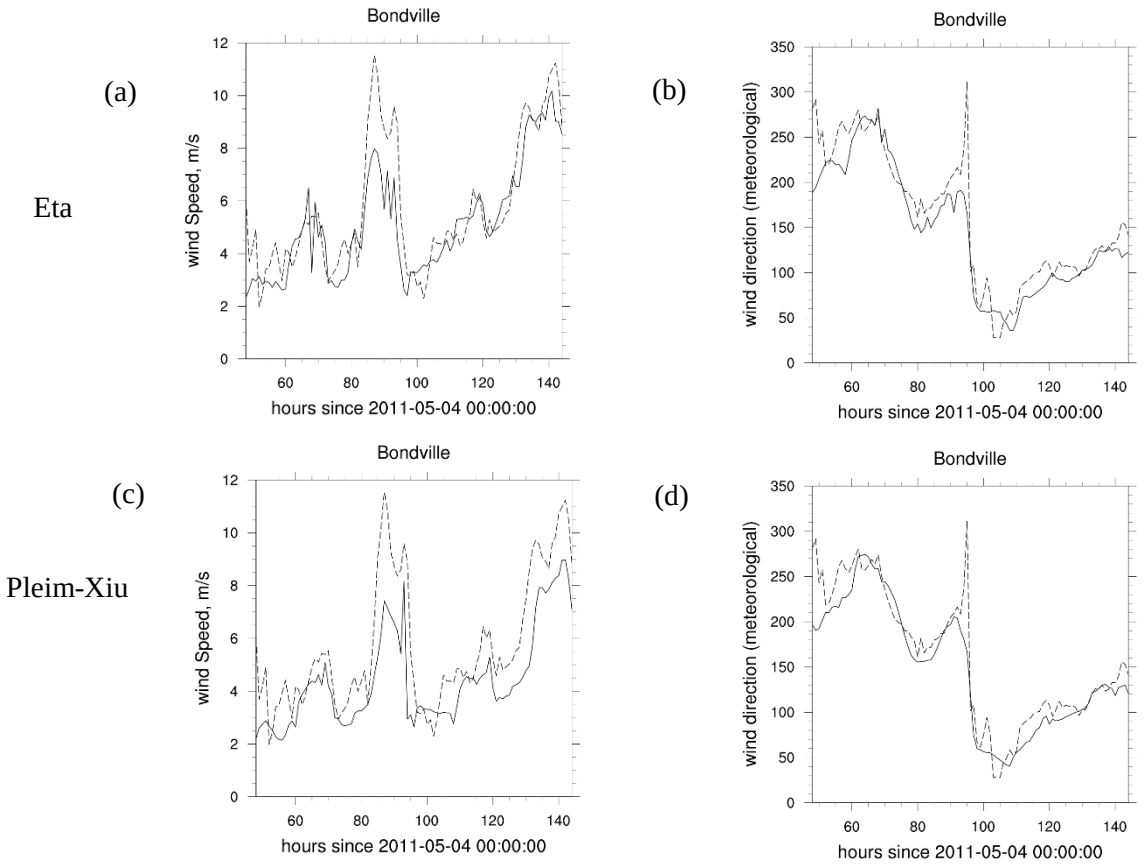

Figure 3.1 Time series plot (a, b, c, d from left to right, top to bottom) of wind speed wind direction in Bondville for Eta and Pleim-Xiu schemes in surface layer stage. Solid line: WRF simulation, dashed line: WARM observation data.

As to the Monin-Obukhov and Pleim-Xiu schemes, Monin-Obukhov has a slightly better statistic performance, but the difference is small (Table 3.4). Considering the importance of the surface physics (surface layer, land surface model and planetary boundary layer) in WRF (Figure 1.5), no optimum scheme was selected. A combined test of land surface model and planetary boundary layer was conducted in section 3.4. The Pleim-Xiu scheme in surface layer was chosen to pair the Pleim-Xiu scheme in land surface model due to the fact that they were developed by the same research group and were tested together by the WRF team (Wang et al., 2016).

Table 3.4 Statistics from DS337.0 and MADIS in surface layer stage.*

		Temp (K)		SH (g/kg)	UGRD (m/s)		VGRD (m/s)	
Statistic	Scheme	DS337	MADIS	DS337	DS337	MADIS	DS337	MADIS
RMSE	Monin-Obukhov	**2.39**	**2.13**	**1.31**	**1.61**	**1.57**	**1.69**	**1.69**
	Eta	2.5	2.17	1.41	*2.14*	*2.04*	*2.24*	*2.18*
	Pleim-Xiu	2.45	2.2	1.33	1.63	1.61	1.73	1.74
MB	Monin-Obukhov	*-1.00*	*-0.82*	**0.52**	**0.05**	**0.03**	-0.13	-0.08
	Eta	***-0.85***	***-0.66***	0.66	-0.34	-0.35	0.2	0.17
	Pleim-Xiu	*-1.01*	*-0.82*	0.53	0.08	0.04	**-0.07**	**-0.01**
GE	Monin-Obukhov	**1.85**	1.7	**0.90**	**1.21**	**1.19**	**1.24**	**1.21**
	Eta	1.86	**1.68**	0.97	1.51	1.47	1.49	1.46
	Pleim-Xiu	1.91	1.77	0.91	1.23	1.22	1.27	1.25
IOA	Monin-Obukhov	**0.97**	**0.97**	**0.95**	**0.94**	**0.94**	**0.88**	**0.88**
	Eta	0.96	0.97	0.94	0.92	0.91	0.84	0.84
	Pleim-Xiu	0.97	0.97	0.95	0.94	0.93	0.88	0.88

** red and italic: out of the benchmark range, bold: best value identified*

Table 3.5 Aggregated daily and hourly statistics from WARM ground monitoring station data in surface layer stage stage. Daily and Hourly columns have been compiled using measurements from all 19 WARM stations.*

	Daily		**Hourly**		**Bondville**	
Scheme	Eta	Pleim-Xiu	Eta	Pleim-Xiu	Eta	Pleim-Xiu
T2 (K)						
MB	**-0.38**	*-0.59*	**-0.49**	*-0.65*	0.31	**0.18**
RMSE	**0.99**	1.00	2.03	**1.96**	1.32	**1.28**
GE	**0.66**	0.71	**1.47**	1.50	**1.05**	1.06
IOA	**0.97**	0.97	0.96	**0.97**	0.98	**0.98**
CC	0.96	**0.97**	0.93	**0.95**	**0.97**	0.97
RH (%)						
MB	3.78	**3.66**	4.29	**4.03**	**-3.56**	-4.00
RMSE	6.73	**6.17**	10.93	**10.09**	8.40	**8.31**
GE	5.16	**4.94**	7.90	**7.85**	**5.86**	5.99
IOA	0.77	**0.79**	0.91	**0.92**	0.93	**0.93**
CC	0.69	**0.75**	0.84	**0.87**	0.91	**0.92**
WS10 (m/s)						
MB	*0.77*	**0.17**	*1.04*	**0.27**	***-0.59***	*-1.30*
RMSE	1.26	**1.00**	*2.03*	**1.56**	**1.33**	1.76
GE	0.99	**0.77**	1.54	**1.24**	**0.97**	1.38
IOA	0.76	**0.79**	0.78	**0.82**	**0.91**	0.84
CC	0.70	**0.70**	0.69	**0.72**	0.88	**0.89**
Pres(Pa)						
MB			**118.34**	140.66	**80.37**	97.48
RMSE			**237.04**	237.70	**130.57**	132.99
GE			183.98	**182.91**	**110.28**	111.13
IOA			**0.96**	0.96	**0.92**	0.92
CC			0.94	**0.95**	0.91	**0.93**
WDir10 (°)						
MB	*-10.87*	**-9.65**	***-10.66***	*-11.45*	*-15.03*	***-13.49***
RMSE	**27.64**	28.08	37.11	**33.25**	29.09	**27.57**
GE	21.98	**21.04**	24.89	**22.62**	20.35	**18.29**
IOA	**0.95**	0.95	0.94	**0.95**	0.96	**0.96**
CC	**0.92**	0.91	0.90	**0.92**	0.94	**0.94**

** red and italic: out of the benchmark range, bold: best value identified*

3.3 Microphysics

In this stage, the WRF Single-Moment 6-class (WSM6) scheme, the Lin et al. (Lin) scheme, the Eta microphysics and the Thompson et al. (Thompson) scheme were considered.

Table 3.6 Physics options design table in microphysics stage.

Physics category to test	Micro-physics	Longwave radiation	Shortwave radiation	Surface layer	Land surface model	Planetary boundary layer	Cumulus
Micro-physics	WSM6	RRTM	Dudhia	Pleim-Xiu	Pleim-Xiu	ACM2	KF,turn off
	Lin	RRTM	Dudhia	Pleim-Xiu	Pleim-Xiu	ACM2	KF,turn off
	Eta	RRTM	Dudhia	Pleim-Xiu	Pleim-Xiu	ACM2	KF,turn off
	Thompson	RRTM	Dudhia	Pleim-Xiu	Pleim-Xiu	ACM2	KF,turn off

From the MET results (Table 3.7), only small differences were observed in RH or wind speed among these four different schemes. RMSE of UGRD ranged from 1.63 m/s to 1.64 m/s for DS 337.0 and 1.60 m/s to 1.61 m/s for MADIS. RMSE of SH ranged from 1.33 g/kg to 1.55 g/kg. With respect to temperature, the WSM6 scheme performed better in RMSE and GE, but not in MB compared with Eta. As discussed earlier, RMSE and IOA weigh more than MB in terms of reliability. So WSM6 was preferred in this comparison.

In site results (Table 3.8), the WSM6 scheme was better at predicting wind speed and pressure, although with only slight advantages. For RH and T2, there was a clear trend that the WSM6 scheme was better at hourly scale and the Eta scheme at daily scale. Considering CAMx and SMOKE model needs WRF output at hourly scale, the WSM6 was selected in the remaining stages.

Table 3.7 Statistics from DS337.0 and MADIS in microphysics stage.*

		Temp (K)		***SH (g/kg)***	***UGRD (m/s)***		***VGRD (m/s)***	
Statistic	Scheme	DS337	MADIS	DS337	DS337	MADIS	DS337	MADIS
RMSE	WSM6	**2.45**	**2.20**	**1.33**	1.63	1.61	1.73	1.74
	Lin	2.51	2.29	1.33	1.64	1.61	1.71	1.73
	Eta	2.51	2.31	1.34	**1.63**	1.60	**1.70**	**1.73**
	Thompson	2.57	2.37	1.35	1.63	**1.60**	1.72	1.73
MB	WSM6	*-1.01*	***-0.82***	0.53	0.08	0.04	-0.07	-0.01
	Lin	*-1.05*	*-0.89*	**0.52**	0.09	0.04	-0.07	**0.00**
	Eta	***-0.98***	*-0.83*	0.53	0.09	0.04	**-0.05**	0.00
	Thompson	*-1.06*	*-0.90*	0.53	**0.08**	**0.03**	-0.06	0.01
GE	WSM6	**1.91**	**1.77**	**0.91**	1.23	1.22	1.27	1.25
	Lin	1.98	1.85	0.91	1.24	1.22	1.26	1.25
	Eta	1.96	1.86	0.92	**1.23**	1.22	**1.25**	**1.24**
	Thompson	*2.00*	1.91	0.92	1.24	**1.22**	1.26	1.25
IOA	WSM6	**0.97**	**0.97**	**0.95**	0.94	0.93	0.88	0.88
	Lin	0.96	0.97	0.94	0.94	0.94	0.88	0.88
	Eta	0.96	0.97	0.94	**0.94**	**0.94**	**0.88**	**0.88**
	Thompson	0.96	0.96	0.94	0.94	0.94	0.88	0.88

** red and italic: out of the benchmark range, bold: best value identified*

Table 3.8 Aggregated daily and hourly statistics from WARM ground monitoring station data in microphysics stage. Daily and Hourly columns have been compiled using measurements from all 19 WARM stations.*

	Daily				Hourly			
Scheme	WSM6	Lin	Eta	Thom-pson	WSM6	Lin	Eta	Thom-pson
T2 (K)								
MB	*-0.59*	*-0.64*	***-0.57***	*-0.66*	***-0.65***	*-0.72*	*-0.66*	*-0.74*
RMSE	1.00	1.03	**0.99**	1.04	**1.96**	2.05	2.06	2.08
GE	0.71	0.74	**0.70**	0.75	**1.50**	1.59	1.60	1.61
IOA	0.97	0.97	**0.97**	0.97	**0.97**	0.97	0.97	0.97
CC	0.97	0.97	**0.97**	0.97	**0.95**	0.94	0.94	0.94
RH (%)								
MB	3.66	3.77	**3.59**	3.96	**4.03**	4.22	4.03	4.42
RMSE	6.17	6.20	**6.08**	6.28	**10.09**	10.36	10.34	10.41
GE	4.94	4.97	**4.83**	4.99	**7.85**	8.10	8.10	8.17
IOA	0.79	0.79	**0.80**	0.79	**0.92**	0.92	0.92	0.92
CC	0.75	0.75	0.75	**0.76**	**0.87**	0.87	0.87	0.87
WS10 (m/s)								
MB	**0.17**	0.19	0.21	0.20	**0.27**	0.29	0.30	0.29
RMSE	**1.00**	1.01	1.01	1.00	**1.56**	1.57	1.57	1.57
GE	**0.77**	0.78	0.79	0.78	**1.24**	1.25	1.25	1.25
IOA	**0.79**	0.78	0.78	0.79	**0.82**	0.82	0.82	0.82
CC	**0.70**	0.70	0.69	0.70	**0.72**	0.72	0.72	0.72
Pres(Pa)								
MB					**140.66**	140.78	143.49	143.62
RMSE					**237.70**	237.86	239.75	240.08
GE					**182.91**	183.08	184.79	185.18
IOA					**0.96**	0.96	0.96	0.96
CC					**0.95**	0.95	0.95	0.95
WDir10 (°)								
MB	-9.65	-9.44	**-9.26**	-9.30	*-11.45*	*-11.41*	*-11.24*	***-11.07***
RMSE	28.08	28.01	28.02	**27.93**	33.25	32.89	**32.81**	33.07
GE	21.04	**20.95**	21.11	20.96	22.62	22.36	**22.36**	22.45
IOA	0.95	0.95	0.95	**0.95**	0.95	0.95	**0.95**	0.95
CC	0.91	0.91	0.91	**0.91**	0.92	0.92	**0.92**	0.92

** red and italic: out of the benchmark range, bold: best value identified*

3.4 Land Surface Model and Planetary Boundary Layer

The Noah Land Surface Model (Noah) and the Pleim-Xiu Land Surface Model (Pleim-Xiu) were considered for the land surface model, and the Asymmetric Convective Model (ACM2), the Yonsei University scheme (YSU) and the Mellor-Yamada-Janjic scheme (MYJ) scheme were chosen for the planetary boundary layer, which gave 6 different combinations. The MYJ scheme in the planetary boundary layer must be run in conjunction with the Eta scheme in the surface layer (Skamarock et al., 2008), whereas the other two schemes do not have such restriction. In this section, when referring to a specific case, the pair "Land Surface Model – Planetary Boundary Layer" was used. For example, PX-ACM2 is the first case in this stage.

Table 3.9 Physics options design table in land surface model and planetary boundary layer stage.

Physics category to test	**Micro-physics**	**Longwave radiation**	**Shortwave radiation**	**Surface layer**	**Land surface model**	**Planetary boundary layer**	**Cumulus**
Land Surface Model	WSM6	RRTM	Dudhia	Pleim-Xiu	Pleim-Xiu	ACM2	KF,turn off
	WSM6	RRTM	Dudhia	Monin-Obukhov	Noah	ACM2	KF,turn off
Planetary Boundary Layer	WSM6	RRTM	Dudhia	Monin-Obukhov	Noah	YSU	KF,turn off
	WSM6	RRTM	Dudhia	Eta	Noah	MYJ	KF,turn off
	WSM6	RRTM	Dudhia	Pleim-Xiu	Pleim-Xiu	YSU	KF,turn off
	WSM6	RRTM	Dudhia	Eta	Pleim-Xiu	MYJ	KF,turn off

Improvement of temperature prediction was observed when changing the land surface model from Pleim-Xiu to Noah, with a 0.37 K MB decrease and 0.44 K RMSE decrease of the MET results in average (Table 3.11), and such improvement was also confirmed in both site daily and hourly results, to a lesser extent though (Table 3.12). This decrease made MB of temperature fall within the benchmark value range (MB < ±0.5 K). In addition, the Noah scheme had similar

performance to the Pleim-Xiu scheme in RH and wind speed/direction. So the Noah scheme outperformed the Pleim-Xiu scheme in Midwest USA.

As to the planetary boundary layer schemes, MYJ, ACM2 and YSU had their own strengths and weaknesses (Table 3.11, Table 3.12). MYJ had the best statistics in temperature and pressure, but worst in wind speed and humidity (both specific humidity and relative humidity). The RMSE of hourly wind speed for MYJ was 2.00 m/s, which was bad compared with 1.57 m/s for ACM2 and 1.54 m/s for YSU. For the other two schemes, ACM2 was better at predicting humidity while YSU was better at wind speed. Table 3.10 summarizes the comparison of these three schemes and Figure 3.2 illustrates the corresponding daily scatter plots of these three schemes with the Noah scheme in the land surface model. Scatter plot of wind speed with MYJ also showed a clear over-prediction trend. ACM2 and YSU were better than MYJ in their own weaknesses, which made both of them preferred candidates in this stage. Considering ACM2 had more advantages in humidity (RMSE of hourly relative humidity for ACM2 was 8.46% compared with 8.73% for YSU) than YSU had in wind speed (RMSE of wind speed for YSU was 1.54 m/s compared with 1.57 m/s for ACM2), the Noah-ACM2 was selected in the land surface model and planetary boundary layer stage. We can also draw the conclusion that temperature is most sensitive to the land surface model and the planetary boundary layer compared to other physics categories evaluated above due to the big improvement when changing the land surface model to the Noah scheme and the planetary boundary layer to the MYJ scheme.

Table 3.10 Summary of comparison in planetary boundary layer stage (> means better than).

Statistic term	Comparison from best to worst
Temperature	MYJ > YSU > ACM2
Humidity	ACM2 > YSU > MYJ
Wind speed	YSU > ACM2 > MYJ
Pressure	MYJ > ACM2 > YSU
Wind direction	ACM2 > YSU > MYJ

Table 3.11 Statistics from DS337.0 and MADIS in land surface model and planetary boundary layer stage.*

		T2 (K)		SH (g/kg)	UGRD (m/s)		VGRD (m/s)	
Statistic	scheme	DS337	MADIS	DS337	DS337	MADIS	DS337	MADIS
RMSE	PX-ACM2	2.45	2.20	**1.33**	1.63	1.61	1.73	1.74
	Noah-ACM2	1.98	1.79	1.55	**1.58**	1.55	**1.65**	**1.66**
	Noah-YSU	**1.96**	1.77	1.60	1.59	**1.54**	1.67	1.66
	Noah-MYJ	2.00	**1.71**	1.66	1.82	1.82	1.84	1.87
	PX-YSU	2.41	2.13	1.36	1.61	1.56	1.69	1.69
	PX-MYJ	2.50	2.17	1.41	*2.14*	*2.04*	*2.24*	*2.18*
MB	PX-ACM2	*-1.01*	*-0.82*	**0.53**	*0.08*	0.04	-0.07	**-0.01**
	Noah-ACM2	*-0.55*	*-0.54*	0.83	-0.05	-0.06	**-0.05**	-0.04
	Noah-YSU	-0.49	-0.51	0.88	**-0.04**	-0.05	-0.08	-0.06
	Noah-MYJ	**-0.46**	**-0.19**	*1.00*	-0.39	-0.37	0.27	0.28
	PX-YSU	*-0.90*	*-0.74*	0.58	0.04	**-0.01**	-0.13	-0.10
	PX-MYJ	*-0.85*	*-0.66*	0.66	-0.34	-0.35	0.20	0.17
GE	PX-ACM2	1.91	1.77	**0.91**	1.23	1.22	1.27	1.25
	Noah-ACM2	1.41	1.41	1.09	**1.19**	1.17	**1.21**	**1.19**
	Noah-YSU	**1.39**	1.39	1.13	1.20	**1.17**	1.22	1.19
	Noah-MYJ	1.43	**1.32**	1.20	1.36	1.36	1.34	1.34
	PX-YSU	1.87	1.71	0.93	1.21	1.18	1.23	1.21
	PX-MYJ	1.86	1.68	0.97	1.51	1.47	1.49	1.46
IOA	PX-ACM2	0.97	0.97	**0.95**	0.94	0.93	0.88	0.88
	Noah-ACM2	0.98	0.98	0.93	**0.94**	0.94	**0.89**	**0.89**
	Noah-YSU	**0.98**	0.98	0.92	0.94	**0.94**	0.89	0.89
	Noah-MYJ	0.97	**0.98**	0.92	0.94	0.93	0.89	0.88
	PX-YSU	0.97	0.97	0.94	0.94	0.94	0.88	0.88
	PX-MYJ	0.96	0.97	0.94	0.92	0.91	0.84	0.84

** red and italic: out of the benchmark range, bold: best value identified*

Table 3.12 Aggregated daily and hourly statistics from WARM ground monitoring station data in land surface model and planetary boundary layer stage. Daily and Hourly columns have been compiled using measurements from all 19 WARM stations.*

	Daily					
Scheme	PX-ACM2	Noah-ACM2	Noah-YSU	Noah-MYJ	PX-YSU	PX-MYJ
T2 (K)						
MB	*-0.59*	*-0.51*	-0.49	**-0.16**	*-0.53*	-0.38
RMSE	1.00	0.96	0.95	**0.75**	0.98	0.99
GE	0.71	0.73	0.71	**0.56**	0.69	0.66
IOA	0.97	0.97	0.98	**0.98**	0.97	0.97
CC	0.97	0.96	0.96	**0.97**	0.97	0.96
RH (%)						
MB	3.66	**3.58**	4.00	4.18	3.69	3.78
RMSE	6.17	**5.92**	6.32	6.53	6.39	6.73
GE	**4.94**	5.02	5.30	5.34	5.19	5.16
IOA	0.79	**0.80**	0.78	0.76	0.78	0.77
CC	0.75	**0.77**	0.75	0.74	0.73	0.69
WS10 (m/s)						
MB	0.17	0.06	0.03	*0.83*	**-0.02**	0.77
RMSE	1.00	1.01	0.98	1.32	**0.96**	1.26
GE	0.77	0.77	0.75	1.04	**0.73**	0.99
IOA	0.79	0.79	0.80	0.74	**0.81**	0.76
CC	0.70	0.68	0.70	0.67	**0.72**	0.70
WDir10 (°)						
MB	-9.65	-9.24	**-8.68**	*-10.67*	-8.83	*10.87*
RMSE	28.08	27.72	27.90	**27.52**	28.10	27.64
GE	21.04	**21.01**	21.31	22.24	21.03	21.98
IOA	0.95	0.95	0.95	**0.95**	0.95	0.95
CC	0.91	0.91	0.91	**0.92**	0.91	0.92

** red and italic: out of the benchmark range, bold: best value identified*

Table 3.12 (cont.) Aggregated daily and hourly statistics from WARM ground monitoring station data in land surface model and planetary boundary layer stage. Daily and Hourly columns have been compiled using measurements from all 19 WARM stations.*

	Hourly					
Scheme	PX-ACM2	Noah-ACM2	Noah-YSU	Noah-MYJ	PX-YSU	PX-MYJ
T2 (K)						
MB	*-0.65*	-0.40	-0.39	**-0.15**	*-0.60*	-0.49
RMSE	1.96	1.63	1.61	**1.54**	1.93	2.03
GE	1.50	1.17	1.16	**1.13**	1.49	1.47
IOA	0.97	0.98	0.98	**0.98**	0.97	0.96
CC	0.95	0.96	0.96	**0.96**	0.95	0.93
RH (%)						
MB	4.03	**3.21**	3.59	4.03	4.13	4.29
RMSE	10.09	**8.46**	8.73	9.46	10.05	10.93
GE	7.85	**6.44**	6.64	7.33	7.88	7.90
IOA	0.92	**0.93**	0.92	0.91	0.92	0.91
CC	0.87	**0.90**	0.90	0.88	0.87	0.84
WS10 (m/s)						
MB	0.27	0.23	0.18	*1.05*	**0.08**	*1.04*
RMSE	1.56	1.57	1.54	*2.00*	**1.53**	2.03
GE	1.24	1.21	1.19	1.57	**1.18**	1.54
IOA	0.82	0.84	**0.84**	0.78	0.84	0.78
CC	0.72	0.72	**0.73**	0.69	0.73	0.69
Pres(Pa)						
MB	140.7	137.3	146.2	**115.9**	146.7	118.3
RMSE	237.7	234.1	241.4	**228.3**	243.7	237.0
GE	182.9	179.2	185.6	**176.2**	188.3	184.0
IOA	0.96	0.96	0.96	**0.96**	0.96	0.96
CC	0.95	**0.95**	0.95	0.94	0.95	0.94
WDir10 (°)						
MB	*-11.45*	*-10.33*	*-10.51*	***-10.02***	*-10.89*	*-10.66*
RMSE	33.25	**32.53**	32.56	34.72	32.56	37.11
GE	22.62	**21.90**	21.95	23.51	22.04	24.89
IOA	0.95	0.95	0.95	0.95	**0.95**	0.94
CC	0.92	0.92	0.92	0.91	**0.92**	0.90

** red and italic: out of the benchmark range, bold: best value identified*

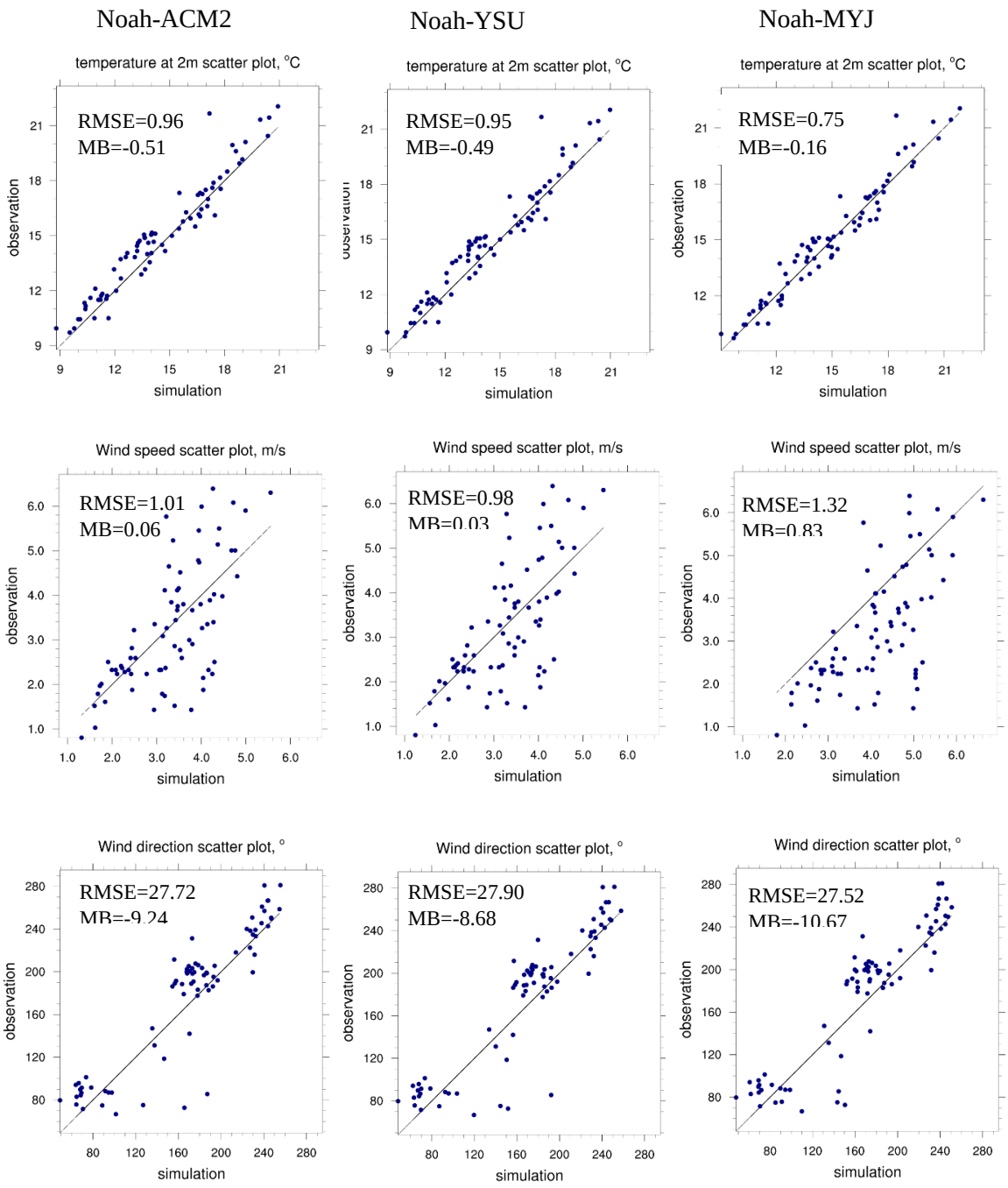

Figure 3.2 Scatter plots of aggregated (19 IL WARM stations) daily temperature, wind speed and wind direction (from top to bottom) in the planetary boundary layer stage (ACM2, YSU and MYJ from left to right). The solid line indicates 1:1 equivalent line.

3.5 Radiation

In this stage, the Rapid Radiative Transfer Model (RRTM) scheme, the RRTMg scheme, and the Goddard scheme were considered in longwave radiation, and the Dudhia scheme and the RRTMg scheme were considered in shortwave radiation. The longwave and shortwave radiation in WRF are used for calculating atmospheric heat for the ground heat budget by radiative flux divergence and surface downward radiation (Skamarock et al., 2008). So temperature is closely related to the radiation schemes and should be paid more attention when determining the best case. In this stage, four combinations of longwave and shortwave radiation were used: RRTM-Dudhia (R.-Dud.), RRTMg-Dudhia (R.g-Dud.), Goddard-Dudhia (G.-Dud.), and RRTMg-RRTMg (R.g-R.g), with the denotation of Longwave radiation–Shortwave radiation.

Table 3.13 Physics schemes design table in radiation stage.

Physics category to test	**Micro-physics**	**Long wave radiation**	**Short wave radiation**	**Surface layer**	**Land surface model**	**Planetary boundary layer**	**Cumulus**
Long wave radiation	WSM6	RRTM	Dudhia	Monin-Obukhov	Noah	ACM2	KF,turn off
	WSM6	RRTMg	Dudhia	Monin-Obukhov	Noah	ACM2	KF,turn off
Short wave radiation	WSM6	Goddard	Dudhia	Monin-Obukhov	Noah	ACM2	KF,turn off
	WSM6	RRTMg	RRTMg	Monin-Obukhov	Noah	ACM2	KF,turn off

RRTMg-RRTMg was observed to provide the best performance of all the four statistical terms (RMSE, MB, GE and IOA) in temperature, relative humidity and pressure in both MET and site results, except the hourly temperature statistics. It was also the only case that every statistic term of all the weather parameters was within the benchmark value range. Figure 3.4 shows the scatter plots of aggregated daily temperature for RRTM-Dudhia, Goddard-Dudhia, and RRTMg-RRTMg. As to wind speed and wind direction, the statistics were close between the four cases. The RMSE of hourly wind speed ranged from 1.55 m/s to 1.57 m/s, and the GE varied from 1.20

m/s to 1.21 m/s. According to the WRF users' guide (Wang et al., 2016), the RRTMg scheme is an improved version of the RRTM scheme developed in 2009, with the use of Monte Carlo Independent Column Approximation method of random cloud overlap, and the results in this thesis indeed showed the improved overall performance. The RRTMg-RRTMg case was chosen as the final optimum case.

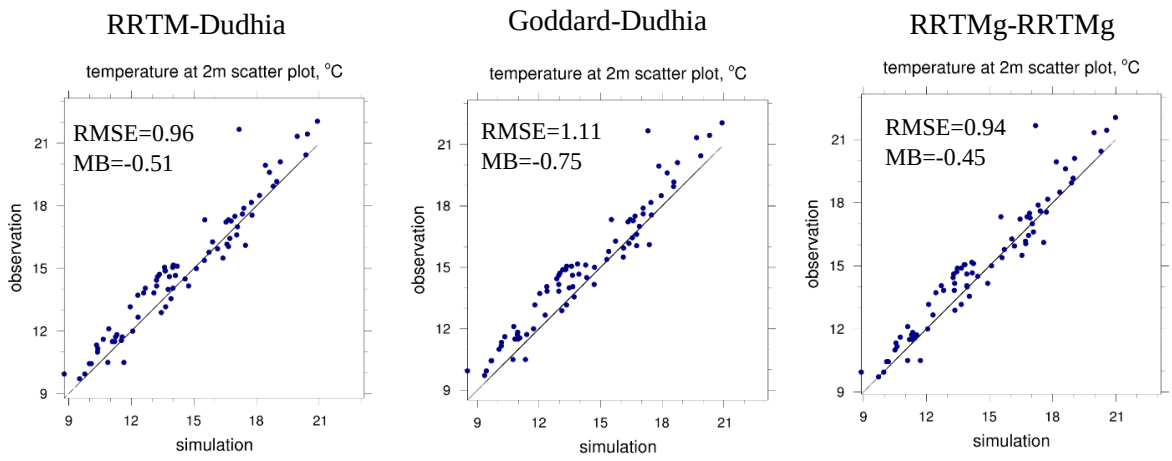

Figure 3.3 Scatter plots of aggregated (19 IL WARM stations) daily temperature in the radiation stage. The solid line in scatter plots indicates 1:1 equivalent line.

Table 3.14 Statistics from DS377.0 and MADIS in radiation stage.*

		T2 (K)		SH (g/kg)	UGRD (m/s)		VGRD (m/s)	
Statistic	Scheme	DS337	MADIS	DS337	DS337	MADIS	DS337	MADIS
RMSE	RRTM-Dudhia	1.98	1.79	1.55	1.58	1.55	1.65	1.66
	RRTMg-Dudhia	2.06	1.87	1.54	1.58	1.55	1.65	1.66
	Goddard-Dudhia	2.11	1.91	1.54	1.59	1.55	1.65	**1.66**
	RRTMg-RRTMg	**1.89**	**1.78**	**1.53**	**1.57**	**1.55**	**1.64**	1.66
MB	RRTM-Dudhia	*-0.55*	*-0.54*	0.83	-0.05	-0.06	-0.05	-0.04
	RRTMg-Dudhia	*-0.69*	*-0.69*	0.80	**-0.04**	**-0.05**	-0.07	-0.05
	Goddard-Dudhia	*-0.80*	*-0.78*	**0.78**	-0.05	-0.06	-0.07	-0.05
	RRTMg-RRTMg	**-0.23**	**-0.47**	0.84	-0.05	-0.06	**0.02**	**-0.03**
GE	RRTM-Dudhia	1.41	1.41	1.09	1.19	1.17	1.21	1.19
	RRTMg-Dudhia	1.49	1.48	1.08	1.19	1.17	1.21	1.19
	Goddard-Dudhia	1.53	1.51	**1.08**	1.20	1.17	1.21	**1.19**
	RRTMg-RRTMg	**1.32**	**1.40**	1.09	**1.18**	**1.17**	**1.20**	1.19
IOA	RRTM-Dudhia	0.98	0.98	0.93	0.94	0.94	0.89	0.89
	RRTMg-Dudhia	0.97	0.98	0.93	0.94	0.94	0.89	0.89
	Goddard-Dudhia	0.97	0.98	0.93	0.94	0.94	0.89	0.89
	RRTMg-RRTMg	**0.98**	**0.98**	**0.93**	**0.95**	**0.94**	**0.90**	**0.89**

** red and italic: out of the benchmark range, bold: best value identified*

Table 3.15 Aggregated daily and hourly statistics from WARM ground monitoring station data in radiation stage. Daily and Hourly columns have been compiled using measurements from all 19 WARM stations.*

	Daily				Hourly			
Scheme	R.-Dud.	R.g-Dud.	G.-Dud.	R.g-R.g	R.-Dud.	R.g-Dud.	G.-Dud.	R.g-R.g
T2 (K)								
MB	*-0.51*	*-0.66*	*-0.75*	**-0.45**	-0.40	*-0.56*	*-0.63*	**-0.36**
RMSE	0.96	1.06	1.11	**0.94**	**1.63**	1.70	1.71	1.64
GE	0.73	0.83	0.89	**0.70**	**1.17**	1.24	1.26	1.18
IOA	0.97	0.97	0.97	**0.98**	**0.98**	0.97	0.97	0.98
CC	0.96	0.96	**0.96**	0.96	**0.96**	0.96	0.96	0.96
RH (%)								
MB	3.58	3.95	3.97	**3.33**	3.21	3.57	3.58	**2.98**
RMSE	5.92	6.23	6.14	**5.82**	8.46	8.74	8.64	**8.29**
GE	5.02	5.25	5.16	**4.93**	6.44	6.65	6.62	**6.35**
IOA	0.80	0.78	0.79	**0.81**	0.93	0.92	0.93	**0.93**
CC.	0.77	0.76	**0.78**	0.77	0.90	0.90	0.90	**0.90**
WS10 (m/s)								
MB	0.06	0.02	**0.02**	0.08	0.23	0.19	**0.18**	0.26
RMSE	1.01	**1.00**	1.00	1.01	1.57	1.56	**1.55**	1.57
GE	0.77	**0.76**	0.77	0.77	1.21	1.20	**1.20**	1.21
IOA	0.79	0.79	0.79	**0.80**	0.84	0.84	**0.84**	0.84
CC	0.68	**0.69**	0.69	0.68	0.72	0.72	**0.73**	0.72
Pres(Pa)								
MB					**137.28**	137.53	138.47	137.83
RMSE					234.14	234.38	235.09	**234.11**
GE					179.22	179.58	180.06	**179.21**
IOA					0.96	0.96	0.96	**0.96**
CC					0.95	0.95	0.95	**0.95**
WDir10 (°)								
MB	-9.24	**-9.15**	-9.45	-9.32	*-10.33*	*-10.17*	*-10.66*	**-9.85**
RMSE	27.72	27.06	27.02	**26.89**	32.53	**32.49**	32.84	32.76
GE	21.01	20.63	20.95	**20.55**	21.90	**21.91**	22.04	21.90
IOA	0.95	0.95	0.95	**0.95**	0.95	**0.95**	0.95	0.95
CC	0.91	0.92	0.92	**0.92**	0.92	**0.92**	0.92	0.92

** red and italic: out of the benchmark range, bold: best value identified*

3.6 Optimum Case

The optimum case was achieved after optimizing each stage. Table 3.16 lists the physics configuration of the optimum case and the starting case. Table 3.17 shows the results of the optimum case from Borge's study (2008) and corresponding values in this thesis for reference. Tables 3.18 and 3.19 show the complete statistical results of these two cases.

Table 3.16 Optimum case and base case physics configurations.

Case	Micro physics	Longwave radiation	Shortwave radiation	Surface layer	Land surface model	Planetary boundary layer	Cumulus
Starting	WSM6	RRTM	Dudhia	Monin-Obukhov	Pleim-Xiu	ACM2	KF
Optimum	WSM6	RRTMg	RRTMg	Monin-Obukhov	Noah	ACM2	KF, turn off

The optimum case has a clear improvement in temperature, while preserving decent ability to simulate wind. In fact, the only difference of the physics configurations between the starting case and the optimum case are the radiation group and surface physics group, which directly influences heat fluxes and temperature calculation (Table 1.1). When applying the same physics configuration to Oct case (simulation period from Oct 25, 2011 to Oct 30, 2011), the WRF model still gave a reasonable simulation skill. For the October case, although the wind direction statistics was not as good as the May case, the wind speed was better, with the RMSE of hourly wind speed equal to 1.35 m/s compared with the 1.57 m/s for the May case. Temperature and pressure statistics became worse, while humidity was better. Therefore, the optimum case found in the sensitivity analysis of May can also be applied in October.

Table 3.17 Best case statistics from Borge et al. (2008) and corresponding values from this thesis.*

Variables	**T2 (K)**			**WS10 (m/s)**			**WDir10 (°)**		**SH (g/kg)**		
Statistics	MB	GE	IOA	MB	RMSE	IOA	MB	GE	MB	GE	IOA
Borge	**0.16**	*2.17*	0.9	**-0.07**	*2.40*	0.72	*-22.62*	*60.67*	-0.29	1.63	0.63
May	-0.36	**1.18**	**0.98**	0.26	1.57	0.84	-9.85	**21.90**	0.84	1.09	0.93
Oct	-0.18	1.41	0.95	0.40	**1.35**	**0.86**	**-5.76**	*30.02*	**0.11**	**0.32**	**0.97**

** red and italic: out of the benchmark range, bold: best value identified*

Table 3.18 Statistics from DS377.0 and MADIS for the starting case, the optimum May case and the October case.*

		T2 (K)		**SH (g/kg)**	**UGRD (m/s)**		**VGRD (m/s)**	
Statistic	Scheme	DS337	MADIS	DS337	DS337	MADIS	DS337	MADIS
RMSE	Starting	2.42	2.14	1.34	1.61	1.57	1.69	1.69
	Optimum	**1.89**	**1.78**	1.53	1.57	1.55	1.64	1.66
	Oct	2.10	1.81	**0.45**	**1.50**	**1.16**	**1.31**	**1.27**
MB	Starting	*-1.02*	*-0.84*	0.54	0.05	**0.02**	-0.13	-0.08
	Optimum	**-0.23**	**-0.47**	0.84	-0.05	-0.06	**0.02**	**-0.03**
	Oct	*-0.69*	*-0.65*	**0.11**	**0.04**	0.05	-0.04	-0.03
GE	Starting	1.87	1.71	0.91	1.21	1.19	1.23	1.20
	Optimum	**1.32**	**1.40**	1.09	1.18	1.17	1.20	1.19
	Oct	1.43	1.39	**0.32**	**0.89**	**0.88**	**0.93**	**0.96**
IOA	Starting	0.97	0.97	0.94	0.94	0.94	0.88	0.88
	Optimum	**0.98**	**0.98**	0.93	**0.95**	**0.94**	0.90	0.89
	Oct	0.96	0.96	**0.97**	0.86	0.90	**0.94**	**0.94**

** red and italic: out of the benchmark range, bold: best value identified*

Table 3.19 Aggregated daily and hourly statistics from WARM data for the starting case, the optimum case and the October case.*

	Daily			Hourly		
Scheme	Starting	Optimum	Oct	Starting	Optimum	Oct
T2 (K)						
MB	*-0.65*	-0.45	**0.21**	*-0.71*	-0.36	**-0.18**
RMSE	1.03	**0.94**	1.04	1.90	**1.64**	1.90
GE	0.75	**0.70**	0.89	1.45	**1.18**	1.41
IOA	0.97	**0.98**	0.97	0.97	**0.98**	0.95
CC	**0.97**	0.96	0.96	0.95	**0.96**	0.91
RH (%)						
MB	4.04	3.33	**-0.33**	4.42	2.98	**1.26**
RMSE	6.41	5.82	**4.48**	10.05	**8.29**	9.61
GE	5.11	4.93	**3.64**	7.76	**6.35**	7.08
IOA	0.79	0.81	**0.93**	0.92	0.93	**0.94**
CC	0.75	0.77	**0.88**	0.88	**0.90**	0.89
WS10 (m/s)						
MB	**-0.04**	0.08	0.48	**0.09**	0.26	0.40
RMSE	**0.97**	1.01	0.99	1.52	1.57	**1.35**
GE	**0.74**	0.77	0.77	1.17	1.21	**0.99**
IOA	**0.80**	0.80	0.79	0.85	0.84	**0.86**
CC	**0.71**	0.68	0.69	0.74	0.72	**0.77**
Pres(Pa)						
MB				142.13	137.83	**137.57**
RMSE				238.02	**234.11**	303.71
GE				183.07	**179.21**	203.82
IOA				0.96	**0.96**	0.95
CC				0.95	**0.95**	0.92
WDir10 (°)						
MB	-9.89	**-9.32**	-20.93	*-10.72*	-9.85	**-5.76**
RMSE	28.28	**26.89**	63.06	33.02	**32.76**	43.87
GE	21.13	**20.55**	*47.40*	22.46	**21.90**	*30.02*
IOA	0.94	**0.95**	0.82	0.95	**0.95**	0.94
CC	0.91	**0.92**	0.80	0.92	**0.92**	0.90

** red and italic: out of the benchmark range, bold: best value identified*

3.7 Impact of Different Horizontal Resolutions

Both the coarse domain (12 km grid size) and the fine domain (4 km grid size) were examined, with the same optimum physics configuration. The results suggested that the coarse domain outperformed the fine domain in nearly all the statistic terms, except MB of some variables, as shown in Table 3.20. The finding is in agreement with previous studies, as discussed in the introduction 1.2.2. Considering computational efficiency, the coarse domain is preferred when using WRF as a weather simulation model.

However, it does not necessarily mean the coarse domain WRF output is better than the fine domain one as CTM inputs. WRF output variables are stored in a gridded format, while traditional verification methods use station observational data. In order to match a point in a grid domain, interpolation like bilinear and distance-weighted mean or simply choosing the nearest neighbor (used in this thesis) is common practice. But no matter what method is used, there is no perfect way to evaluate the model performance grid by grid with point observation data. Therefore, the traditional verification methods are limited for evaluating the WRF model as CTM inputs. To find out the answer of this question, similar approaches could be adopted by applying WRF output into CTMs and comparing CTM outputs with pollutants of interest, which is beyond the scope of this thesis.

Table 3.20 Aggregated daily and hourly statistics from WARM data for the coarse domain and the fine domain with the optimum physics configuration.*

	Daily		**Hourly**	
Horizontal resolution	Coarse	Fine	Coarse	Fine
T2 (K)				
MB	-0.45	**-0.45**	**-0.34**	-0.36
RMSE	**0.81**	0.94	**1.40**	1.64
GE	**0.64**	0.70	**1.09**	1.18
IOA	**0.98**	0.98	**0.98**	0.98
CC	**0.98**	0.96	**0.97**	0.96
RH (%)				
MB	3.44	**3.33**	3.18	**2.98**
RMSE	**5.45**	5.82	**7.91**	8.29
GE	**4.55**	4.93	**6.11**	6.35
IOA	**0.83**	0.81	**0.94**	0.93
CC	**0.83**	0.77	**0.92**	0.90
WS10 (m/s)				
MB	**0.06**	0.08	**0.24**	0.26
RMSE	**1.00**	1.01	**1.57**	1.57
GE	**0.76**	0.77	**1.20**	1.21
IOA	**0.80**	0.80	**0.84**	0.84
CC	**0.69**	0.68	**0.73**	0.72
Pres(Pa)				
MB			**116.27**	137.83
RMSE			**194.24**	234.11
GE			**158.29**	179.21
IOA			**0.97**	0.96
CC			**0.97**	0.95
WDir10 (°)				
MB	**-8.99**	-9.32	-9.88	**-9.85**
RMSE	**25.93**	26.89	**32.56**	32.76
GE	**19.85**	20.55	**21.67**	21.90
IOA	**0.95**	0.95	**0.95**	0.95
CC	**0.92**	0.92	**0.92**	0.92

** bold: better value identified*

CHAPTER 4: SUMMARY

` In this thesis, a sensitivity analysis including 17 WRF runs was conducted to explore the optimum physics configuration for the Midwest USA in May 2011, with the grid size of 12 km for the coarse domain and 4 km for the nested domain. The model output was compared with observation data, including DS337.0 data, MADIS data and WARM data. The NCL and MET software packages were used to post-process the WRF output. In order to evaluate the model performance. MB, RMSE, GE, IOA and CC were the chosen statistics and benchmark values from previous MM5 studies were used as reference. After the sensitivity analysis was finished, the same optimum physics configuration was tested for October 2011 to examine the applicability in different seasons. Finally, outputs from both 12 km and 4 km domain were compared to investigate the impact of different spatial resolutions.

The focus of this thesis was to discuss a general approach to conduct sensitivity analysis over a specific region and provide a guideline for choosing the optimum physics configuration in WRF for the Midwest USA, with the purpose of using WRF out as input to the chemical transport model CAMx. Currently researchers tend to use different ways for the sensitivity analysis based on their understanding. The method used in this thesis looked into all the physics categories in WRF and moved into a stage wise fashion rather than picking certain combinations. By performing sensitivity analysis in stages also helped to determine the strengths and weaknesses for different schemes in the same physics category. For example, in the planetary boundary layer stage, the MYJ scheme was found to simulate more accurately temperature (hourly RMSE = 1.54 K compared with RMSE = 1.64 K for the optimum case), but had poorer performance with wind speed (hourly RMSE = 2.00 m/s compared with RMSE = 1.57 m/s for the optimum case). In addition, different physics categories also had different impact on certain weather variables. For

example, the wind speed was not sensitive to the shortwave and longwave radiation since hourly RMSE changed less than 0.02 m/s and GE changed less than 0.01 m/s. The wind speed, however, was sensitive to planetary boundary layer where there was nearly 0.5 m/s difference between the best case and the worst case when changing planetary boundary layer schemes. Similarly, temperature was more sensitive to the land surface model, the planetary boundary layer and the radiation. Statistical results showed that the optimum case was acceptable to use in CTMs based on benchmarking from past studies. All the daily and hourly statistical terms were within the benchmark value range for the May case, and only the GE of wind direction and the MB of temperature were out of the benchmark value range for the October case. Compared with a previous study by Borge et al. (2008), the results presented in this thesis appear consistent. The coarse domain (12 km grid size) output and the fine domain (4 km grid size) output were evaluated and the results supported the previous studies that coarse domain outperformed the fine domain. However, this cannot lead to the conclusion that the fine domain output is inappropriate for use in current CTMs because the usual method of using point measurements to compare with grid prediction has its own drawbacks. A complete evaluation would require also evaluation of the CTM results which was not within the scope of this thesis. .

The final optimum physics configuration for the Midwest USA is as follows:

1. Microphysics: WSM6
2. Longwave radiation: RRTMg
3. Shortwave radiation: RRTMg
4. Surface Layer: Monin-Obukhov
5. Land surface model: Noah
6. Planetary boundary layer: ACM2
7. Cumulus: KF for the coarse domain and turned off for the nested domain

Future studies may include both WRF and CTMs to conduct the sensitivity analysis by using the same methods but comparing the pollutants concentration as the final evaluation criterion. Also, more weather variables could be added into analysis, including upper air weather observations and precipitations. Due to not using upper air data, not much information was obtained from the microphysics and the cumulus stage. Finally, different matching methods between the grid WRF output and the point observation data like bilinear or distance-weighted mean could be tested to determine which one would be better.

REFERENCES

Aligo, Eric a., William a. Gallus, and Moti Segal. 2009. “On the Impact of WRF Model Vertical Grid Resolution on Midwest Summer Rainfall Forecasts.” *Weather and Forecasting* 24 (2): 575–94.

Appel, K. W., K. M. Foley, J. O. Bash, R. W. Pinder, R. L. Dennis, D. J. Allen, and K. Pickering. 2011. “A Multi-Resolution Assessment of the Community Multiscale Air Quality (CMAQ) Model v4.7 Wet Deposition Estimates for 2002–2006.” *Geoscientific Model Development* 4 (2): 357–71.

Awan, Nauman K., H. Truhetz, and a. Gobiet. 2011. “Parameterization-Induced Error Characteristics of MM5 and WRF Operated in Climate Mode over the Alpine Region: An Ensemble-Based Analysis.” *Journal of Climate* 24 (12): 3107–23.

Baker, A. R., T. Lesworth, C. Adams, T. D. Jickells, and L. Ganzeveld. 2010. “Estimation of atmospheric nutrient inputs to the Atlantic Ocean from 50°N to 50°S based on large-scale field sampling: Fixed nitrogen and dry deposition of phosphorus.” *Global Biogeochemical Cycles* 24(3).

Balasubramanian, Srinidhi, Sotiria Koloutsou-vakakis, D Michael Mcfarland, and Mark J Rood. 2015. “Journal of Geophysical Research : Atmospheres.” *Journal of Geophysical Research: Atmospheres*, 1–15.

Behera, S. N., Sharma, M., Aneja, V. P., and Balasubramanian, R. 2013. “Ammonia in the atmosphere: a review on emission sources, atmospheric chemistry and deposition on terrestrial bodies.” *Environ Sci Pollut Res Int* **20**, 8092-131.

Borge, Rafael, Vassil Alexandrov, Juan José del Vas, Julio Lumbreras, and Encarnacion Rodríguez. 2008. “A Comprehensive Sensitivity Analysis of the WRF Model for Air Quality Applications over the Iberian Peninsula.” *Atmospheric Environment* 42 (37): 8560–74.

Brook, Robert D, Jeffrey R Brook, and Sanjay Rajagopalan. 2003. “Air Pollution: The ‘Heart’ of the Problem.” *Current Hypertension Reports* 5 (1): 32–39.

Brown, David, Debra Baker, Tom Downs, Mike Ku, Winston Hao, Mike Kiss, Nick Witcraft, Matthew Johnson, and Da-Lin Zhang. 2012. “WRF Meteorological Modeling in Support of SIP Regional Air Quality Modeling for Base Year 2007.” Iowa Department of Natural Resources.

Brown, David. 2014. “WRF Meteorological Modeling In Support Of Regional Air Quality Modeling for the 2011 Base Year”. Iowa Department of Natural Resources.

Brunekreef, B. and B. Forsberg. 2005. “Epidemiological Evidence of Effects of Coarse Airborne Particles on Health.” *European Respiratory Journal* 26 (2): 309–18.

Byun, D. W., and J. K. S. Ching, 1999. "Science algorithms of the EPA Models-3 Community Multiscale Air Quality (CMAQ) modeling system." *U.S. Environmental Protection Agency*, Washington, DC, USA.

CMAS. 2015. "SMOKE v3.7 user's manual." *Community Modeling and Analysis System*, https://www.cmascenter.org/smoke.

Coulter. 2004. "EPA-CMB8.2 Users Manual." *U.S. Environmental Protection Agency*, Washington, DC, USA.

Denman, K.L., G. Brasseur, A. Chidthaisong, P. Ciais, P.M. Cox, R.E. Dickinson, D. Hauglustaine, C. Heinze, E. Holland, D. Jacob, U., and 2007 Lohmann, S Ramachandran, P.L. da Silva Dias, S.C. Wofsy and X. Zhang. 2007. "Couplings Between Changes in the Climate System and Biogeochemistry." *Climate Change 2007: The Physical Science Basis. Contribution of Working Group I to the Fourth Assessment Report of the Intergovernmental Panel on Climate Change (IPCC)* 21 (7): 499–587.

Developmental Testbed Center. 2016. "Model Evaluation Tools Version 4.1 (METv4.1) User's Guide 4.1." Boulder, Colorado

Dudhia, Jimy. 2012. "Overview of WRF Physics." *WRF Users' Tutorial 2012*, http://www2.mmm.ucar.edu/wrf/users/tutorial/201301/dudhia_physics.pdf.

Emery, Chris, Edward Tai, and Greg Yarwood. 2001. "Enhanced Meteorological Modeling and Performance Evaluation for Two Texas Ozone Episodes." *Environ International Corporation*, 235.

Environ. 2014. "User's Guide COMPREHENSIVE AIR QUALITY MODEL WITH EXTENSIONS Version 6.1." *ENVIRON International Corporation*, Novato, California, USA.

Erisman, J. W., a. Bleeker, J. Galloway, and M. S. Sutton. 2007. "Reduced Nitrogen in Ecology and the Environment." *Environmental Pollution* 150 (1): 140–49.

Erisman, Jan Willem, James N Galloway, Sybil Seitzinger, Albert Bleeker, Nancy B Dise, A M Roxana Petrescu, Allison M Leach, and W. de Vries. 2013. "Consequences of Human Modification of the Global Nitrogen Cycle." *Philosophical Transactions of the Royal Society B: Biological Sciences* 368 (1621). doi:10.1098/rstb.2013.0116.

Galloway, James N., John D. Aber, Jan Willem Erisman, Sybil P. Seitzinger, Robert W. Howarth, Ellis B. Cowling, and B. Jack Cosby. 2003. "The Nitrogen Cascade." *BioScience* 53 (4): 341.

Galloway, James N, Alan R Townsend, Jan Willem Erisman, Mateete Bekunda, Zucong Cai, John R Freney, Luiz a Martinelli, Sybil P Seitzinger, and Mark a Sutton. 2008. "Transformation of the Nitrogen Cycle: Recent Trends, Questions, and Potential Solutions." *Science (New York, N.Y.)* 320 (5878): 889–92.

Gao, Wenlong, Hao Yang, Liang Kou, and Shenggong Li. 2015. “Effects of Nitrogen Deposition and Fertilization on N Transformations in Forest Soils: A Review.” *Journal of Soils and Sediments* 15 (4): 863–79.

Gilliland, A. B., K. W. Appel, R. W. Pinder, and R. L. Dennis. 2006. “Seasonal NH3 emissions for the continental united states: Inverse model estimation and evaluation,” *Atmospheric Environment*, 40(26): 4986-4998.

Grell, G. A., Dudhia, Jimy, and Stauffer, David R.. 1994. “A Description of the Fifth-Generation Penn State/NCAR Mesoscale Model (MM5).” *NCAR Technical Note NCAR/TN-398+STR*, no. December: 121.

Illinois State Water Survey (ISWS). 2016. “Water and Atmospheric Resources Monitoring (WARM) Program – Data Access”. http://www.isws.illinois.edu/warm/weather/. Apr. 2016

Jacob, D. J. 1999. “Introduction to Atmospheric Chemistry.” *Princeton University Press*, Princeton, New Jersey

Li, Laifang, Wenhong Li, and Jiming Jin. 2014. “Improvements in WRF Simulation Skills of Southeastern United States Summer Rainfall: Physical Parameterization and Horizontal Resolution.” *Climate Dynamics* 43 (7-8): 2077–91.

Mass, Clifford F., David Ovens, Ken Westrick, and Brian A. Colle. 2002. “Does Increasing Horizontal Resolution Produce More Skillful Forecasts? The Results of Two Years of Real-Time Numerical Weather Prediction over the Pacific Northwest.” *Bulletin of the American Meteorological Society* 83 (3): 407–430.

Mcnally, Dennis E, Ft Wright, and Craig Tremback. 2002. “MM5 METEOROLOGICAL MODEL OVER THE CONTINENTAL UNITED STATES : Protocol for Annual and Episodic Evaluation Task Order 4TCG-68027015 Prepared for : Mr . Pat Dolwick Office of Air Quality Planning and Standards U . S . Environmental Protection Agency Researc.” *Reports*, no. July 2002.

Moriasi, D.N., J.G. Arnold, M.W. Van Liew, R.L. Binger, R.D. Harmel, and T.L. Veith. 2007. “Model Evaluation Guidelines for Systematic Quantification of Accuracy in Watershed Simulations.” *Transactions of the ASABE* 50 (3): 885–900.

National Centers for Environmental Prediction (NCEP)/National Weather Service/NOAA/U.S. Department of Commerce. 2008, updated daily. “NCEP ADP Global Upper Air and Surface Weather Observations (PREPBUFR format), May 1997 - Continuing.” *Research Data Archive at the National Center for Atmospheric Research, Computational and Information Systems Laboratory*, Data – Access http://rda.ucar.edu/datasets/ds337.0/. Apr 2016a

National Centers for Environmental Prediction (NCEP). 2015. “METAR Data – Data Access” https://madis.noaa.gov/madis_metar.shtml. Apr, 2016b

National Oceanic and Atmospheric Administration (NOAA). 2016. “North American Mesoscale (NAM) data from National Operational Model Archive & Distribution System – Data Access.” http://nomads.ncdc.noaa.gov/data.php?name=access#hires_weather_datasets. Apr, 2016

Noble, Erik, Leonard M. Druyan, and Matthew Fulakeza. 2014. “The Sensitivity of WRF Daily Summertime Simulations over West Africa to Alternative Parameterizations. Part I: African Wave Circulation.” *Monthly Weather Review* 142 (4): 1588–1608.

Pannell, David J. 1997. “Sensitivity Analysis of Normative Economic Models: Theoretical Framework and Practical Strategies.” *Agricultural Economics* 16 (2): 139–52.

Pérez, J. C., J. P. Díaz, A. González, J. Expósito, F. Rivera-López, and D. Taima. 2014. “Evaluation of WRF Parameterizations for Dynamical Downscaling in the Canary Islands.” *Journal of Climate* 27 (14): 5611–31. doi:10.1175/JCLI-D-13-00458.1.

Pope III, C Arden, Richard T Burnett, Michael J Thun, Eugenia E Calle, Daniel Krewski, and George D Thurston. 2002. “Lung Cancer, Cardiopulmonary Mortality, and Long-Term Exposure to Fine Particulate Air Pollution.” *The Journal of the American Medical* 287 (9).

Pope, C Arden, Majid Ezzati, Douglas W Dockery, C A Pope III, Majid Ezzati, and Douglas W Dockery. 2009. “Fine-Particulate Air Pollution and Life Expectancy in the United States.” *New England Journal of Medicine* 360 (4): 376–86.

Queen, Ashley, and Yang Zhang. 2008. “Examining the Sensitivity of MM5–CMAQ Predictions to Explicit Microphysics Schemes and Horizontal Grid Resolutions, Part III—The Impact of Horizontal Grid Resolution.” *Atmospheric Environment* 42 (16): 3869–81.

Ravishankara, A.R., Daniel, J.S., Portmann, R.W. 2009. “Nitrous oxide (N2O): The dominant ozone-depleting substance emitted in the 21st century.” *Science* 326 (5949): 123-125.

Renard, Jean J., Sheryl E. Calidonna, and Michael V. Henley. 2004. “Fate of Ammonia in the Atmosphere - A Review for Applicability to Hazardous Releases.” *Journal of Hazardous Materials* 108 (1-2): 29–60.

Ribaudo, Marc, Jorge Delgado, Leroy Hansen, Michael Livingston, Roberto Mosheim, and James Williamson. 2011. “Nitrogen in Agricultural Systems: Implications for Conservation Policy.” *Environmental Protection*, no. 127: 89.

Roebber, Paul J, and David M Schultz. 2004. “Towards Improved Prediction : High-Resolution and Ensemble Modeling Systems in Operations” 2003 (October 2003).

Smil, Vaclav. 1999. “Nitrogen in Crop Production: An Account of Global Flows.” *Global Biogeochemical Cycles* 13 (2): 647.

Smil, Vaclav. 2002. “Nitrogen and Food Production: Proteins for Human Diets.” *Ambio* 31 (2): 126–31.

Spiro, Thomas, and William Stigliani. “Chemistry of the Environment.” *Upper Saddle River*, New Jersey: Prentice Hall, 2003.

The NCAR Command Language (Version 6.3.0) [Software]. 2016. Boulder, Colorado: UCAR/NCAR/CISL/TDD. http://dx.doi.org/10.5065/D6WD3XH5.

UCAR. 2016. “WRF Mesoscale Model Users homepage - Data Access.” http://www2.mmm.ucar.edu/wrf/users/download/get_sources_wps_geog.html, Last accessed April 2016

University of North Carolina (UNC), Community Modeling and Analysis System. 2012. “Operational Guidance for the Community Multiscale Air Quality (CMAQ) Modeling SystemVersion 5.0.” Chapel Hill, North Carolina, USA

U.S. Environmental Protection Agency. 2011. “Reactive Nitrogen in the United States: An Analysis of Inputs, Flows, Consequences, and Management Options. A Report of the EPA Science Advisory Board.” *U.S. Environmental Protection Agency*, Washington, DC, USA,

U.S. Environmental Protection Agency. 2014. “Modeling Guidance for Demonstrating Attainment of Air Quality Goals for Ozone, PM2s, and Regional Haze.” *U.S. Environmental Protection Agency*, Washington, DC, USA,

U.S. Environmental Protection Agency. 2016. "Air Quality Models | Support Center for Regulatory Atmospheric Modeling (SCRAM) " US *U.S. Environmental Protection Agency*, Washington, DC, USA, https://www3.epa.gov/ttn/scram/aqmindex.htm

U.S. Environmental Protection Agency. 2016. “Nitrous Oxide Emissions | Climate Change.” *U.S. Environmental Protection Agency*, Washington, DC, USA, http://epa.gov/climatechange/ghgemissions/gases/n2o.html

Vitousek, P.M., John D Aber, Robert W Howarth, and Gene E Likens. 1997. “Human Alteration of the Global Nitrogen Cycle: Causes and Consequences.” *Issues in Ecology* 1: 1–17.

Watson. 1979. “Chemical element balance receptor model methodology for assessing the sources of fine and total particulate matter in Portland, Oregon.” Ph.D. Dissertation. Oregon Graduate Center, Beaverton, OR.

Wilmot, C M, B Rappenglück, X Li, and G Cuchiara. 2014. “MM5 v3.6.1 and WRF v3.5.1 Model Comparison of Standard and Surface Energy Variables in the Development of the Planetary Boundary Layer,” no. 2006: 2693–2707.

Wang, W., et al.. 2016. “WRF-ARW Version 3 Modeling System User’s Guide.” *WRF-ARW website*.

Yu, Shaocai, Rohit Mathur, Jonathan Pleim, George Pouliot, David Wong, Brian Eder, Kenneth Schere, Rob Gilliam, and S. Trivikrama Rao. 2012a. “Comparative Evaluation of the Impact of WRF-NMM and WRF-ARW Meteorology on CMAQ Simulations for O3 and Related Species during the 2006 TexAQS/GoMACCS Campaign.” *Atmospheric Pollution Research* 3 (April): 149–62.

Yu, S., R. Mathur, J. Pleim, G. Pouliot, D. Wong, B. Eder, K. Schere, R. Gilliam, and S. T. Rao. 2012b. “Comparative Evaluation of the Impact of WRF/NMM and WRF/ARW Meteorology on CMAQ Simulations for $PM_{2.5}$ and Its Related Precursors during the 2006 TexAQS/GoMACCS Study.” *Atmospheric Chemistry and Physics* 12 (9): 4091–4106.

Yu, Xingna, Jia Ma, Junlin An, Liang Yuan, Bin Zhu, Duanyang Liu, Jing Wang, Yang Yang, and Huxiong Cui. 2016. “Impacts of Meteorological Condition and Aerosol Chemical Compositions on Visibility Impairment in Nanjing, China.” *Journal of Cleaner Production* 131. Elsevier Ltd: 112–20

Zhang, Yang, Ping Liu, Betty Pun, and Christian Seigneur. 2006. “A Comprehensive Performance Evaluation of MM5-CMAQ for the summer 1999 Southern Oxidants Study episode—Part I: Evaluation Protocols, Databases, and Meteorological Predictions.” *Atmospheric Environment* 40 (26): 4825–38.

Zhang, Yang, Joshua Hemperly, Nicholas Meskhidze, and William C Skamarock. 2012. “The Global Weather Research and Forecasting (GWRF) Model : Model Evaluation , Sensitivity Study , and Future Year Simulation.” *Atmospheric and Climate Sciences* 2 (July): 231–53. doi:10.4236/acs.2012.23024.

Zhang, Hongliang, Gang Chen, Jianlin Hu, Shu-Hua Chen, Christine Wiedinmyer, Michael Kleeman, and Qi Ying. 2014. “Evaluation of a Seven-Year Air Quality Simulation Using the Weather Research and Forecasting (WRF)/Community Multiscale Air Quality (CMAQ) Models in the Eastern United States.” *The Science of the Total Environment* 473-474 (March). Elsevier B.V.: 275–85.

APPENDIX A: WRF NAMELIST FILES

WPS namelist

```
&share
 wrf_core = 'ARW',
 max_dom = 2,
 start_date = '2011-05-04_00:00:00','2011-05-04_00:00:00',
 end_date = '2011-05-10_00:00:00','2011-05-10_00:00:00',
 interval_seconds = 21600
 io_form_geogrid = 2,
 debug_level=200
/

&geogrid
 parent_id = 1, 1,
 parent_grid_ratio = 1, 3,
 i_parent_start = 1, 245,
 j_parent_start = 1, 156,
 e_we = 481, 253,
 e_sn =  369, 181,
 geog_data_res = '5m','2m',
 dx = 12000.0,
 dy = 12000.0,
 map_proj = 'lambert',
 ref_lat = 40.0000000000,
 ref_lon = -97.0000000000,
 truelat1 = 33.0000000000,
 truelat2 = 45.0000000000,
 stand_lon = -97.0000000000,
 geog_data_path = '/data/kanfu2/WRF/data/geog'
 opt_geogrid_tbl_path = '/data/kanfu2/WRF/WRF3.5.1/WPS/geogrid/'
/

&ungrib
 out_format = 'WPS',
 prefix = 'FILE',
/

&metgrid
 fg_name = 'FILE','SST'
 io_form_metgrid = 2,
 opt_metgrid_tbl_path = '/data/kanfu2/WRF/WRF3.5.1/WPS/metgrid/'
```

OBSGRID namelist

```
&record1
 start_year               =  2011     !update
 start_month               =    04     !update
 start_day                =    15     !update
 start_hour               =    00     !update
 end_year                 =  2011     !update
 end_month                 =    05     !update
 end_day                  =    20     !update
 end_hour                 =    00     !update
 interval                 = 21600
/

&record2
 grid_id                  = 1         !run it twice for both domains
 obs_filename              = '/data/kanfu2/WRF/data/oneyear/OBSGRID/obs'  ! update oneyear to
TARGET
 remove_data_above_qc_flag   = 32768
 remove_unverified_data      = .TRUE.
/
 trim_domain               = .FALSE.
 trim_value                = 5

&record3
 max_number_of_obs          = 120000
 fatal_if_exceed_max_obs     = .TRUE.
/

&record4
 qc_test_error_max          = .TRUE.
 qc_test_buddy              = .TRUE.
 qc_test_vert_consistency    = .TRUE.
 qc_test_convective_adj      = .TRUE.
 max_error_t                = 5
 max_error_uv               = 5
 max_error_z                = 8
 max_error_rh               = 20
 max_error_p                = 600
 max_buddy_t                = 8
 max_buddy_uv               = 8
 max_buddy_z                = 8
 max_buddy_rh               = 40
 max_buddy_p                = 800
 buddy_weight               = 1.0
 max_p_extend_t             = 1300
max_p_extend_w              = 1300
/

&record5
 print_obs_files            = .TRUE.
```

```
 print_found_obs            = .FALSE.
 print_header               = .FALSE.
 print_analysis             = .FALSE.
 print_qc_vert              = .FALSE.
 print_qc_dry               = .FALSE.
 print_error_max            = .FALSE.
 print_buddy                = .FALSE.
 print_oa                   = .FALSE.
/

&record7
 use_first_guess            = .TRUE.
 f4d                        = .TRUE.
 intf4d                     =  21600
 lagtem                     = .FALSE.
/

&record8
 smooth_type                =  1
 smooth_sfc_wind            =  0
 smooth_sfc_temp            =  0
 smooth_sfc_rh              =  0
 smooth_sfc_slp             =  0
 smooth_upper_wind          =  0
 smooth_upper_temp          =  0
 smooth_upper_rh            =  0
/

&record9
 oa_type                    = 'Cressman'
 radius_influence           = 0,
 mqd_minimum_num_obs        = 30
 mqd_maximum_num_obs        = 1000
 oa_min_switch              = .TRUE.
oa_max_switch               = .TRUE.
/
 oa_type                    = 'MQD'
 oa_3D_option               = 1
 oa_3D_type                 = 'Cressman'
 radius_influence           = 5,4,3,2,


&plot_sounding
 file_type                  = 'raw'
 read_metoa                 = .TRUE.
/
 file_type                  = 'used'
```

WRF namelist

```
&time_control
run_days = 6,
run_hours = 0,
run_minutes = 0,
run_seconds = 0,
start_year = 2011, 2011,
start_month = 05, 05,
start_day = 04, 04,
start_hour = 00, 00,
start_minute = 00, 00,
start_second = 00, 00,
end_year = 2011, 2011,
end_month = 05, 05,
end_day = 10, 10,
end_hour = 00, 00,
end_minute = 00, 00,
end_second = 00, 00,
interval_seconds = 21600
input_from_file = .true.,.true.,
fine_input_stream = 0,0,
history_interval = 60, 60,
frames_per_outfile = 1000, 1000,
restart = .false.,
restart_interval = 5000,
io_form_history = 2
io_form_restart = 2
io_form_input = 2
io_form_boundary = 2
debug_level = 200
auxinput1_inname = "metoa_em.d<domain>.<date>"
auxinput4_inname = "wrflowinp_d<domain>",
auxinput4_interval = 360,
io_form_auxinput4 = 2,
/

&domains
time_step = 72,
max_dom = 2,
s_we = 1, 1,
e_we = 481, 253,
s_sn = 1, 1,
e_sn =  369, 181,
s_vert = 1, 1,
e_vert = 30, 30,
num_metgrid_levels = 40
dx = 12000, 4000,
dy = 12000, 4000,
grid_id = 1, 2,
parent_id = 1, 1,
```

```
i_parent_start = 1, 245
j_parent_start = 1, 156
parent_grid_ratio = 1, 3,
parent_time_step_ratio = 1, 3,
feedback = 1,
smooth_option = 0
/
&fdda
grid_fdda = 1, 1,
gfdda_inname = "wrffdda_d<domain>",
gfdda_end_h = 144, 144,
gfdda_interval_m = 360, 360,
fgdt = 0, 0,
if_no_pbl_nudging_uv = 1, 1,
if_no_pbl_nudging_t = 1, 1,
if_no_pbl_nudging_q = 1, 1,
if_zfac_uv = 0, 0,
k_zfac_uv = 10, 10,
if_zfac_t = 0, 0,
k_zfac_t = 10, 10,
if_zfac_q = 0, 0,
k_zfac_q = 10, 10,
guv = 0.0003, 0.0003,
gt = 0.0003, 0.0003,
gq = 0.0003, 0.0003,
if_ramping = 0,
dtramp_min = 60.0,
io_form_gfdda = 2,
grid_sfdda = 1, 1,
sgfdda_inname = "wrfsfdda_d<domain>",
sgfdda_end_h = 144, 144,
sgfdda_interval_m = 360, 360,
io_form_sgfdda = 2,
guv_sfc = 0.0003, 0.0003,
gt_sfc = 0.0003, 0.0003,
gq_sfc = 0.0003, 0.0003,
rinblw = 250.,

/
&physics
mp_physics = 6, 6,        !WSM6
ra_lw_physics = 4, 4,     !RRTMg
mp_zero_out = 2,
ra_sw_physics = 4, 4,     !RRTMg
radt = 12, 12,
sf_sfclay_physics = 1, 1,          !MM5
sf_surface_physics = 2, 2,         !Noah
num_soil_layers = 4,
bl_pbl_physics = 7, 7,             !ACM2
bldt = 0, 0, 0,
cu_physics = 1, 0,                 !KF
```

```
cudt = 5, 5,
sst_update = 1,
isfflx = 1,
icloud = 1,
num_land_cat = 24,
slope_rad = 1,
topo_shading = 1,
shadlen = 25000.,
/

&dynamics
w_damping = 1,
diff_opt = 1,
km_opt = 4,
diff_6th_opt = 2, 2,
diff_6th_factor = 0.12, 0,12
base_temp = 290.
damp_opt = 3,
zdamp = 5000., 5000.,
dampcoef = 0.2, 0.2,
khdif = 0, 0,
kvdif = 0, 0,
non_hydrostatic = .true., .true.,
moist_adv_opt = 1,
scalar_adv_opt = 1,
/

&bdy_control
spec_bdy_width = 5,
spec_zone = 1,
relax_zone = 4,
specified = .true., .false.,
nested = .false., .true.,
/

&namelist_quilt
nio_tasks_per_group = 0,
nio_groups = 1,
/
```